Infield Self-Calibration of Intrinsic Parameters for Two Rigidly Connected IMUs

(Supplementary material for ICRA submission [2783])

Can Huang, Wenqian Lai, Ruonan Guo, and Kejian J. Wu

XREAL, Inc. Email: {canhuang,wqlai,rnguo,kejian}@xreal.com

Abstract

This paper presents a study on the infield self-calibration of two rigidly connected IMUs' intrinsic parameters, without the aid of any external sensors, equipment, or specialized procedures. Specifically, we consider the calibration of gyroscope biases, gyroscope scale factors, and accelerometer biases, using only IMU data and known extrinsics between the two IMUs. We focus on the observability analysis of this system, and show that all gyroscope intrinsic parameters and a portion of accelerometer biases are observable, with information from both IMUs and sufficient motion. Moreover, we identify the additional unobservable directions in the intrinsic parameters that arise from various degenerate motions. Finally, we validate our observability findings through numerical simulations, and assess our system's calibration accuracy using real-world data.

I. Introduction And Related Work

Inertial Measurement Units (IMUs) are widely adopted for localization across various fields, such as robotics, wearables, smartphones, and autonomous vehicles, due to their 3D motion sensing capabilities and low costs. A plentiful number of navigation systems combine IMU with complementary sensors, such as GNSS [1], [2], camera [3], [4], [5], [6], [7], [8], lidar [9], [10], to improve calibration robustness and accuracy. Some systems [11], [12], [13] employ multiple rigidly connected IMUs to achieve better performance and resilience against sensor failures. However, commercial-grade MEMS IMUs suffer from noises and intrinsic errors (biases, scale factors, axis misalignments). The accuracy of these systems relies heavily on well-calibrated intrinsic parameters of the IMUs. As a result, calibration becomes critical to maintain high performance in IMU systems.

There exist effective techniques for IMU calibration. A widely used approach involves the use of high-precision instruments, such as rate tables [14], [15], optical tracking system [16], [17] or calibration target [18], within controlled factory or laboratory settings. These methods can yield highly accurate calibration results. However, due to the inherent characteristics of low-cost IMU sensors, the calibrated parameters are subject to change or drift over time and device use because of temperature variations, humidity, and mechanical stress, impairing the system's accuracy. Consequently, it is crucial to apply *infield calibration* techniques, which adaptively compute and update the calibration parameters of the IMUs to the latest status, at the user's end.

As for infield calibration, a common strategy involves utilizing additional sensors to simultaneously calibrate both IMU intrinsic and extrinsic parameters. For instance, [19], [20], [21], [22], [23] use visual-inertial information to estimate IMU parameters. [24] estimates lidar-IMU intrinsics and extrinsics within a continuous-time batch optimization framework. However, these configurations typically result in increased system size, power consumption, and processing cost, limiting their applicability across practical scenarios. Even if an additional sensor, such as a camera, is available, adverse environmental factors, including poor lighting, lack of texture, or rapid movement, can degrade calibration accuracy and the overall system's performance. Alternatively, certain IMU *self-calibration* methods [25], [26], [27], [28] can be used to obtain the intrinsic parameters, but they require specialized procedures, such as positioning the sensor on a perfectly stationary platform in multiple different attitudes. As a result, these methods are also challenging to implement for end users, especially in consumer scenarios.

On the other hand, for rigidly connected multi-IMU configurations, it is possible to perform *infield self-calibration* of the IMUs, i.e., without external equipment, auxiliary sensors or specialized procedures, by leveraging only the IMU data and the geometric constraints derived from inter-IMU rigidity [29], [30], [31], [32]. For example, [29], [30], [31] focus solely on extrinsic calibration, but under the assumption of known intrinsic parameters. Meanwhile, both extrinsic rotation and part of intrinsics are estimated in [32], but just for multi-gyroscope systems, ignoring the information from accelerometers. In contrast, in this paper, we study the problem of infield self-calibration of intrinsic parameters of the rigid dual-IMU (RDI) system using *both* gyroscope and accelerometer data, assuming the two IMUs are rigidly connected and their extrinsics are well-calibrated and stay unchanged.

Moreover, one of the main challenges with IMU infield self-calibration systems, when compared to sensor-rich setups or controlled laboratory conditions, is the limited diversity and lack of control over input data, which introduces considerable uncertainty not only in the precision but also in the observability of the estimated calibration parameters. In fact, previous studies have already shown that the observability properties of the visual-inertial navigation systems [22], [33], [34], [35] and

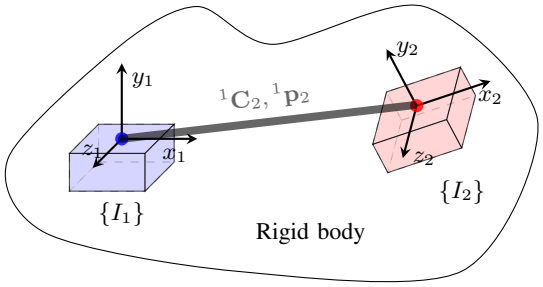

Fig. 1: The RDI system comprises two rigidly connected IMUs, denoted by I_1 and I_2, with constant inter-IMU extrinsic rotation $^1\mathbf{C}_2$ and position $^1\mathbf{p}_2$.

dual-IMU relative localization [36] can alter with different motion patterns, as well as the impact of motion constraints on the accuracy and effectiveness of IMU self-calibration [29], [32]. Therefore, observability analysis of IMU-based systems under different types of motions is necessary, in order to determine whether the estimation results are reliable. In the literature, however, observability properties of the RDI system with intrinsic self-calibration have yet to be explored.

To address the aforementioned limitations, in this paper, we propose a state estimation system for infield intrinsic self-calibration of an RDI platform. Specifically, our system employs measurements derived from inter-IMU extrinsic constraints, which utilize both gyroscope and accelerometer data. We focus on the observability analysis of this system, under sufficient motion as well as special motion constraints, by deriving the system's observability matrix and its corresponding rank condition. The main contributions of this paper are:

- We introduce a self-calibration system for two rigidly connected IMUs' intrinsics, including gyroscope biases, gyroscope scale factors, and accelerometer biases of both IMUs, using only IMU data and inter-IMU extrinsic constraints.
- We prove that, by using information from both gyroscopes and accelerometers of the two IMUs, all intrinsics, except composite accelerometer bias, are observable under sufficient motion. And the corresponding necessary and sufficient motion condition is provided.
- We analytically determine the additional unobservable directions that arise from various degenerate motions, indicated by the motion condition that leads to different ranks of the observability matrix.
- We verify the impact of these unobservable directions on the calibration results through numerical simulations, and demonstrate the effectiveness and accuracy of our proposed RDI intrinsic self-calibration system using real-world data.

II. Rigid Dual IMU State Estimation

This section describes the dynamic and measurement models of our rigid dual-IMU (RDI) intrinsic self-calibration system. This system consists of two IMUs which are rigidly connected and attached to the same body (see Fig. 1), with the inter-IMU extrinsics (relative pose) constant and known.

A. System State and Dynamic Model

Our system estimates the following 18×1 state vector:

$$\mathbf{x} = \begin{bmatrix} \mathbf{b}_{g_1}^\top & \mathbf{b}_{g_2}^\top & \mathbf{s}_{g_1}^\top & \mathbf{s}_{g_2}^\top & \mathbf{b}_{a_1}^\top & \mathbf{b}_{a_2}^\top \end{bmatrix}^\top \tag{1}$$

where $\mathbf{b}_{g_1}$ and $\mathbf{b}_{g_2}$ represent the gyroscope biases of I_1 and I_2, $\mathbf{s}_{g_1}$ and $\mathbf{s}_{g_2}$ are the gyroscope scale factors, and $\mathbf{b}_{a_1}$ and $\mathbf{b}_{a_2}$ denote the accelerometer biases, respectively.

The IMU measurement model of the angular velocity $^{I_n}\boldsymbol{\omega}_m$ and linear acceleration $^{I_n}\mathbf{a}_m$, with $n = 1, 2$ denoting each IMU, are given by:

$$^{I_n}\boldsymbol{\omega}_m(t) = \mathbf{S}_{g_n}\, ^{I_n}\boldsymbol{\omega}(t) + \mathbf{b}_{g_n}(t) + \mathbf{n}_{g_n}(t) \tag{2}$$

$$^{I_n}\mathbf{a}_m(t) = \, ^{I_n}\mathbf{a}(t) + \mathbf{b}_{a_n}(t) + \mathbf{n}_{a_n}(t) \tag{3}$$

where $^{I_n}\boldsymbol{\omega}(t)$ and $^{I_n}\mathbf{a}(t)$ are the true angular velocity and linear acceleration and gravity vector in IMU frame, $^{I_n}\mathbf{a}(t) = {}^{I_n}\mathbf{C}_G(t)(^G\mathbf{a}_{I_n}(t) - {}^G\mathbf{g})$, with In $^{I_n}\mathbf{C}_G(t)$ the rotation matrix of global frame $\{G\}$ wrt IMU frame $\{I_n\}$ at time t, $^G\mathbf{g}$ the known gravitational acceleration. $\mathbf{S}_{g_n}$ is the gyroscope scale matrix, which is a 3×3 diagonal matrix with the gyroscope scale factors $\mathbf{s}_{g_n}$ on its diagonal. $\mathbf{n}_{g_n}(t)$ and $\mathbf{n}_{a_n}(t)$ are noises of gyroscope and accelerometer measurements, modeled as zero-mean white Gaussian noise processes.

In our system, the continuous-time system dynamics are:

$$\begin{aligned} \dot{\mathbf{b}}_{g_1}(t) &= \mathbf{n}_{wg_1} \quad \dot{\mathbf{b}}_{g_2}(t) = \mathbf{n}_{wg_2} \quad \dot{\mathbf{s}}_{g_1}(t) = \mathbf{0}_3 \\ \dot{\mathbf{s}}_{g_2}(t) &= \mathbf{0}_3 \quad \dot{\mathbf{b}}_{a_1}(t) = \mathbf{n}_{wa_1} \quad \dot{\mathbf{b}}_{a_2}(t) = \mathbf{n}_{wa_2} \end{aligned} \tag{4}$$

The IMU biases are modeled as random walks driven by zero-mean, white Gaussian noise $\mathbf{n}_{w_{g_n}}$ and $\mathbf{n}_{w_{a_n}}$. The gyroscope scale factors are assumed to be time-invariant.

B. Continuous-Time State Equation

The continuous-time state equation is given by:

$$\dot{\mathbf{x}}(t) = \mathbf{F}(t)\,\mathbf{x}(t) + \mathbf{G}(t)\,\mathbf{n}(t) \tag{5}$$

where $\mathbf{F}(t)$ is the continuous-time state transition matrix. From (4), we have:

$$\mathbf{F}(t) = \mathbf{0}_{18} \tag{6}$$

$\mathbf{n}$ is a 12×1 noise vector:

$$\mathbf{n} = \begin{bmatrix} \mathbf{n}_{wg_1}^\top & \mathbf{n}_{wg_2}^\top & \mathbf{n}_{wa_1}^\top & \mathbf{n}_{wa_2}^\top \end{bmatrix}^\top \tag{7}$$

and $\mathbf{G}$ is the noise Jacobian matrix:

$$\mathbf{G} = \begin{bmatrix} \mathbf{I}_6 & \mathbf{0}_6 \\ \mathbf{0}_6 & \mathbf{0}_6 \\ \mathbf{0}_6 & \mathbf{I}_6 \end{bmatrix}_{18\times 12}. \tag{8}$$

In additional, the continuous time system noise covariance matrix $\mathbf{Q}_c(t) = E\left[\mathbf{n}(t+\tau)\,\mathbf{n}^\top(t)\right]$.

C. Discrete-Time State Equation

Given that the IMU measurements are acquired at synchronized discrete time intervals, i.e., from t_{k-1} to t_k for any $k = 1, 2, \cdots$, the linearized discrete-time state equation is:

$$\mathbf{x}_k = \mathbf{\Phi}_{k,k-1}\mathbf{x}_{k-1} + \mathbf{w}_{k,k-1} \tag{9}$$

where the $\mathbf{\Phi}_{k,k-1}$ is the discrete-time state transition matrix:

$$\mathbf{\Phi}_{k,k-1} = \mathbf{\Phi}(t_k, t_{k-1}) = \exp\left[\int_{t_{k-1}}^{t_k} \mathbf{F}(\tau)\,d\tau\right] \tag{10}$$

and the zero-mean, white Gaussian noise $\mathbf{w}_{k,k-1}$ follow the discrete-time system noise covariance matrix $\mathbf{Q}_{k,k-1}$:

$$\mathbf{Q}_{k,k-1} = \int_{t_{k-1}}^{t_k} \mathbf{\Phi}(\tau)\,\mathbf{G}(\tau)\,\mathbf{Q}_c\mathbf{G}^\top(\tau)\,\mathbf{\Phi}^\top(\tau)d\tau \tag{11}$$

It is evident that the state transition matrix is:

$$\mathbf{\Phi} = \mathbf{I}_{18} \tag{12}$$

D. Measurement Model

In this system, we assume constant and known extrinsics, i.e., relative pose, between the two IMUs as:

$$\mathbf{C}({}^{I_1}\mathbf{q}_{I_2})(t) \equiv {}^1\mathbf{C}_2 \tag{13}$$

$${}^{I_1}\mathbf{p}_{I_2}(t) \equiv {}^1\mathbf{p}_2, \quad \text{for } \forall\ t \tag{14}$$

where $\mathbf{C}({}^{I_1}\mathbf{q}_{I_2})$ and ${}^{I_1}\mathbf{p}_{I_2}$ represent the relative rotation matrix and translation vector of I_2 w.r.t I_1, respectively. ${}^1\mathbf{C}_2$ is a constant 3×3 rotation matrix, and ${}^1\mathbf{p}_2$ is a constant 3×1 vector, obtained from previous extrinsic calibration process using existing methods (e.g. [17], [18]).

As these extrinsic constraints (13) and (14) are not direct functions of the system state (1), in what follows, we will derive the time derivatives of the relative rotation and translation to get the desired measurement model.

1) Derivative of the relative rotation:

Since ${}^1\mathbf{C}_2$ is constant, from (13), the first-order derivative of $\mathbf{C}({}^{I_1}\mathbf{q}_{I_2})$ can be derived as:

$$\begin{aligned} & \frac{d}{dt}\mathbf{C}({}^{I_1}\mathbf{q}_{I_2}) \equiv \mathbf{0}_3 \\ \Leftrightarrow \quad & \mathbf{h}_q(\mathbf{x}) \triangleq {}^{I_1}\boldsymbol{\omega} - {}^1\mathbf{C}_2\,{}^{I_2}\boldsymbol{\omega} \equiv \mathbf{0}_{3\times 1} \end{aligned} \tag{15}$$

where ${}^{I_n}\boldsymbol{\omega} = \mathbf{S}_{g_n}^{-1}\left({}^{I_n}\boldsymbol{\omega}_m - \mathbf{b}_{g_n} - \mathbf{n}_{g_n}\right),\ n = 1, 2$, according to (2), and $\mathbf{S}_{g_n}$ is invertible in general.

2) Derivative of the relative translation:

Since ${}^{1}\mathbf{p}_2$ is constant, from (14), the first-order derivative of ${}^{I_1}\mathbf{p}_{I_2}$ can be derived as:

$$\begin{aligned}\frac{\mathrm{d}}{\mathrm{d}t}{}^{I_1}\mathbf{p}_{I_2} &= \frac{\mathrm{d}}{\mathrm{d}t}\left({}^{G}\mathbf{R}_{I_1}^{\top}\left({}^{G}\mathbf{p}_{I_2}-{}^{G}\mathbf{p}_{I_1}\right)\right)\\ &= \frac{\mathrm{d}}{\mathrm{d}t}\left({}^{G}\mathbf{R}_{I_1}^{\top}\right)\left({}^{G}\mathbf{p}_{I_2}-{}^{G}\mathbf{p}_{I_1}\right)+{}^{G}\mathbf{R}_{I_1}^{\top}\frac{\mathrm{d}}{\mathrm{d}t}\left({}^{G}\mathbf{p}_{I_2}-{}^{G}\mathbf{p}_{I_1}\right)\\ &= -\lfloor{}^{I_1}\boldsymbol{\omega}\rfloor{}^{G}\mathbf{R}_{I_1}^{\top}\left({}^{G}\mathbf{p}_{I_2}-{}^{G}\mathbf{p}_{I_1}\right)+{}^{G}\mathbf{R}_{I_1}^{\top}\left({}^{G}\mathbf{v}_{I_2}-{}^{G}\mathbf{v}_{I_1}\right)\\ &= -{}^{I_1}\boldsymbol{\omega}\times{}^{1}\mathbf{p}_2+{}^{I_1}\mathbf{v}_{I_2}-{}^{I_1}\mathbf{v}_{I_1}\\ &\equiv \mathbf{0}_{3\times1}\end{aligned} \tag{16}$$

where ${}^{G}\mathbf{R}_{I_1}$ is the rotation matrix of I_1 w.r.t the global frame, ${}^{G}\mathbf{p}_{I_2}$ and ${}^{G}\mathbf{p}_{I_1}$ are the translation vectors of I_2 and I_1 w.r.t the global frame, respectively. ${}^{I_1}\mathbf{v}_{I_1}$ and ${}^{I_1}\mathbf{v}_{I_2}$ are the linear velocities of I_1 and I_2 w.r.t the $\{I_1\}$ frame, respectively. As these variables are not included in the state vector, we further derive the second-order derivative of ${}^{I_1}\mathbf{p}_{I_2}$ as:

$$\begin{aligned}\mathbf{h}_p(\mathbf{x}) \triangleq \frac{\mathrm{d}^2}{\mathrm{d}t^2}{}^{I_1}\mathbf{p}_{I_2} &= -{}^{I_1}\dot{\boldsymbol{\omega}}\times{}^{1}\mathbf{p}_2+\frac{\mathrm{d}}{\mathrm{d}t}({}^{G}\mathbf{R}_{I_1}^{\top}({}^{G}\mathbf{v}_{I_2}-{}^{G}\mathbf{v}_{I_1}))\\ &= -{}^{I_1}\dot{\boldsymbol{\omega}}\times{}^{1}\mathbf{p}_2+\frac{\mathrm{d}}{\mathrm{d}t}({}^{G}\mathbf{R}_{I_1}^{\top})({}^{G}\mathbf{v}_{I_2}-{}^{G}\mathbf{v}_{I_1})+{}^{G}\mathbf{R}_{I_1}^{\top}\frac{\mathrm{d}}{\mathrm{d}t}({}^{G}\mathbf{v}_{I_2}-{}^{G}\mathbf{v}_{I_1})\\ &= -{}^{I_1}\dot{\boldsymbol{\omega}}\times{}^{1}\mathbf{p}_2-{}^{I_1}\boldsymbol{\omega}\times({}^{I_1}\mathbf{v}_{I_2}-{}^{I_2}\mathbf{v}_{I_1})+{}^{G}\mathbf{R}_{I_1}^{\top}({}^{G}\mathbf{a}_{I_2}-{}^{G}\mathbf{a}_{I_1})\\ &= -{}^{I_1}\dot{\boldsymbol{\omega}}\times{}^{1}\mathbf{p}_2-{}^{I_1}\boldsymbol{\omega}\times\left({}^{I_1}\boldsymbol{\omega}\times{}^{1}\mathbf{p}_2\right)+{}^{1}\mathbf{C}_2\,{}^{I_2}\mathbf{a}-{}^{I_1}\mathbf{a}\\ &\equiv \mathbf{0}_{3\times1}.\end{aligned} \tag{17}$$

where ${}^{1}\mathbf{C}_2\,{}^{I_2}\mathbf{a}-{}^{I_1}\mathbf{a}={}^{1}\mathbf{C}_2({}^{I_2}\mathbf{a}_m-\mathbf{b}_{a_2}-\mathbf{n}_{a_2})-({}^{I_1}\mathbf{a}_m-\mathbf{b}_{a_1}-\mathbf{n}_{a_1})$, according to (3).

It is straightforward that, the time-derivative equations (15) and (17), together with the initial conditions, are fully equivalent to the original extrinsic constraints (13)-(14). Now that we have obtained the desired form of equation (15) and (17), which are functions of the system state and IMU data only, the linearized measurement model of our system, at a given time step t_k, can be written as:

$$\begin{bmatrix}\tilde{\mathbf{z}}_{q,k}\\ \tilde{\mathbf{z}}_{p,k}\end{bmatrix}\simeq\mathbf{H}_k\tilde{\mathbf{x}}_k+\begin{bmatrix}\boldsymbol{\eta}_{q,k}\\ \boldsymbol{\eta}_{p,k}\end{bmatrix},\quad\text{with}\quad\mathbf{H}_k=\begin{bmatrix}\mathbf{H}_{q,k}\\ \mathbf{H}_{p,k}\end{bmatrix} \tag{18}$$

where $\tilde{\mathbf{x}}_k=\mathbf{x}_k-\hat{\mathbf{x}}_k$ is the error of the estimate $\hat{\mathbf{x}}_k$ of the state $\mathbf{x}_k$, $\tilde{\mathbf{z}}_k$ is the measurement residual, $\boldsymbol{\eta}_k$ is the linearized measurement noise, and the corresponding measurement Jacobians are:

$$\mathbf{H}_{q,k}=\begin{bmatrix}-\hat{\mathbf{S}}_{g_1}^{-1} & {}^{1}\mathbf{C}_2\hat{\mathbf{S}}_{g_2}^{-1} & -\boldsymbol{\Lambda}({}^{I_1}\hat{\boldsymbol{\omega}}_k)\hat{\mathbf{S}}_{g_1}^{-1} & {}^{1}\mathbf{C}_2\boldsymbol{\Lambda}({}^{I_2}\hat{\boldsymbol{\omega}}_k)\hat{\mathbf{S}}_{g_2}^{-1} & \mathbf{0}_{3\times6}\end{bmatrix} \tag{19}$$

$$\mathbf{H}_{p,k}=-\begin{bmatrix}\mathbf{K}_k\hat{\mathbf{S}}_{g_1}^{-1} & \mathbf{0}_3 & \mathbf{L}_k\hat{\mathbf{S}}_{g_1}^{-1} & \mathbf{0}_3 & -\mathbf{I}_3 & {}^{1}\mathbf{C}_2\end{bmatrix} \tag{20}$$

where ${}^{I_n}\hat{\boldsymbol{\omega}}_k\triangleq\hat{\mathbf{S}}_{g_n}^{-1}\left({}^{I_n}\boldsymbol{\omega}_{m,k}-\hat{\mathbf{b}}_{g_n}\right),n=1,2$, and $\boldsymbol{\Lambda}(\cdot)$ is a diagonal matrix operator, and

$$\mathbf{K}_k\triangleq\lfloor{}^{I_1}\hat{\boldsymbol{\omega}}_k\times{}^{1}\mathbf{p}_2\rfloor+\lfloor{}^{I_1}\hat{\boldsymbol{\omega}}_k\rfloor\lfloor{}^{1}\mathbf{p}_2\rfloor \tag{21}$$

$$\mathbf{L}_k\triangleq\mathbf{K}_k\boldsymbol{\Lambda}({}^{I_1}\hat{\boldsymbol{\omega}}_k)+\lfloor{}^{1}\mathbf{p}_2\rfloor\boldsymbol{\Lambda}({}^{I_1}\dot{\hat{\boldsymbol{\omega}}}_k) \tag{22}$$

Given the derived system dynamic model (9) and measurement model (15) and (17), we can use various estimation frameworks such as the Extended Kalman Filter (EKF) [6] or optimization-based methods [37] to obtain estimates of the intrinsic calibration states in (1).

It is interesting to note that the gravity vector is canceled out in (17) and does not appear in the system's final measurement or dynamic model. Therefore, our system is independent of gravity and can be applied at arbitrary physical locations, without any knowledge of the actual gravity.

III. Observability Analysis

In this section, we perform observability analysis of the RDI intrinsic self-calibration system with dynamic model (9) and measurement model (15) and (17). Our objective is to identify the unobservable and observable directions in the system's state space, and determine the corresponding necessary and sufficient condition.

We follow the standard approach using the observability matrix [38]. Specifically, the observability matrix $\mathbf{M}$ has its k-th block row as $\mathbf{M}_k=\mathbf{H}_k\boldsymbol{\Phi}_{k,1}$, which corresponds to a certain time step k. Since from (9), $\boldsymbol{\Phi}_{k,1}$ is identity for all k, we can apply (18)-(20) to have:

$$\mathbf{M}_k = \mathbf{H}_k = \begin{bmatrix} -\mathbf{S}_{g_1}^{-1} & {}^1\mathbf{C}_2\mathbf{S}_{g_2}^{-1} & -\mathbf{\Lambda}({}^{I_1}\boldsymbol{\omega}_k)\mathbf{S}_{g_1}^{-1} & {}^1\mathbf{C}_2\mathbf{\Lambda}({}^{I_2}\boldsymbol{\omega}_k)\mathbf{S}_{g_2}^{-1} & \mathbf{0}_3 & \mathbf{0}_3 \\ -\mathbf{K}_k\mathbf{S}_{g_1}^{-1} & \mathbf{0}_3 & -\mathbf{L}_k\mathbf{S}_{g_1}^{-1} & \mathbf{0}_3 & \mathbf{I}_3 & -{}^1\mathbf{C}_2 \end{bmatrix}_{6\times 18} \tag{23}$$

Next, we study the rank of the observability matrix $\mathbf{M}$ and its nullspace, which corresponds to the unobservable directions of our system. First, we observe that from (23), $\mathbf{M}_k$ has a specific structure in its last two block columns. Hence, we have the following result.

Theorem 1.1 *The RDI intrinsic self-calibration system has always three unobservable directions as follows:*

$$\mathbf{N}_{\mathbf{b}_a^+} = \begin{bmatrix} \mathbf{0}_{3\times 12} & \mathbf{I}_3 & {}^1\mathbf{C}_2 \end{bmatrix}^\top \tag{24}$$

PROOF From (23)-(24), it is evident that $\mathbf{M}_k\mathbf{N}_{\mathbf{b}_a^+} = \mathbf{0}_{6\times 1}$ for any k. Hence, $\mathbf{N}_{\mathbf{b}_a^+}$ is a nullspace of $\mathbf{M}$.

Remark 1.1 *The unobservable directions $\mathbf{N}_{\mathbf{b}_a^+}$ correspond to the "composite" accelerometer bias, which is defined as 3dof of combined directions of accelerometer biases, $\mathbf{b}_a^+ \triangleq \mathbf{b}_{a_1} + {}^1\mathbf{C}_2\mathbf{b}_{a_2}$. This bias affects only the system's absolute translation.*

The physical interpretation of Theorem 1.1 is that, in our system, only relative pose measurements between the two IMUs are available. Since these measurements do not provide any information about the platform's absolute translation, the composite accelerometer bias remains unobservable. Therefore, the estimates of these bias directions will be unreliable.

We further analyze the rank of the observability matrix $\mathbf{M}$. Specifically, we apply elementary row and column transformations [39] to the matrix $\mathbf{M}$, to obtain its equivalent matrix $\mathbf{M}'$ as (see Appendix I):

$$\mathbf{M}' = \begin{bmatrix} {}^1\mathbf{C}_2 & \mathbf{0}_3 & \mathbf{0}_3 & \mathbf{0}_3 & \mathbf{0}_3 & \mathbf{0}_3 \\ \mathbf{0}_3 & \mathbf{\Lambda}_2 & \mathbf{0}_3 & \mathbf{0}_3 & \mathbf{\Lambda}_1 & \mathbf{0}_3 \\ \mathbf{0}_3 & \mathbf{0}_3 & \mathbf{I}_3 & \mathbf{0}_3 & \mathbf{0}_3 & \mathbf{0}_3 \\ \mathbf{0}_3 & \mathbf{0}_3 & \mathbf{0}_3 & \mathbb{K} & \mathbb{L} & \mathbf{0}_3 \end{bmatrix} \tag{25}$$

where $\mathbf{\Lambda}_1$, $\mathbf{\Lambda}_2$, $\mathbb{K}$ and $\mathbb{L}$ are given by:

$$\mathbf{\Lambda}_1 = \begin{bmatrix} \mathbf{\Lambda}({}^{I_1}\boldsymbol{\omega}_2 - {}^{I_1}\boldsymbol{\omega}_1) \\ \vdots \\ \mathbf{\Lambda}({}^{I_1}\boldsymbol{\omega}_k - {}^{I_1}\boldsymbol{\omega}_1) \\ \vdots \end{bmatrix}, \ \mathbf{\Lambda}_2 = \begin{bmatrix} {}^1\mathbf{C}_2\mathbf{\Lambda}({}^{I_2}\boldsymbol{\omega}_2 - {}^{I_2}\boldsymbol{\omega}_1) \\ \vdots \\ {}^1\mathbf{C}_2\mathbf{\Lambda}({}^{I_2}\boldsymbol{\omega}_k - {}^{I_2}\boldsymbol{\omega}_1) \\ \vdots \end{bmatrix} \tag{26}$$

$$\mathbb{K} = \begin{bmatrix} \mathbf{K}_2 - \mathbf{K}_1 \\ \vdots \\ \mathbf{K}_k - \mathbf{K}_1 \\ \vdots \end{bmatrix}, \qquad \mathbb{L} = \begin{bmatrix} \mathbf{L}_2 - \mathbf{L}_1 \\ \vdots \\ \mathbf{L}_k - \mathbf{L}_1 \\ \vdots \end{bmatrix} \tag{27}$$

The matrix $\mathbf{M}'$ has the same rank as $\mathbf{M}$, with a block upper-triangular structure. Hence, we have the following result.

Theorem 1.2 *The RDI intrinsic self-calibration system has exactly three unobservable directions $\mathbf{N}_{\mathbf{b}_a^+}$, if and only if the following motion condition is satisfied:*

(i) The matrix $\mathbf{\Lambda}_2$ has full column rank, and

(ii) The matrix $[\mathbb{K}, \mathbb{L}]$ has full column rank.

PROOF It is evident that (i)(ii) is equivalent to $rank(\mathbf{M}) = rank(\mathbf{M}') = 15$, i.e., $\mathbf{M}$ has exactly 3dof nullspace.

We notice that $\mathbf{\Lambda}_2$, $\mathbb{K}$, and $\mathbb{L}$ comprise only angular velocity, angular acceleration, and extrinsics. Hence, the necessary and sufficient condition (i) (ii) is determined only by *rotational* motion of the platform. In fact, this condition can be effectively met through adequate physical motion (see Appendix II). In practice, to guarantee the reliability of the intrinsic estimates, it is important to ensure that the motion satisfies this condition and is rich enough. Specifically, for Condition (i), the angular velocity of the two IMUs must vary over time along all the local x, y, and z axes. In addition, for Condition (ii), the platform must not rotate continuously around a single axis that is either parallel or perpendicular to the baseline ${}^1\mathbf{p}_2$ connecting the two IMUs.

Remark 1.2 *The estimation result of the RDI intrinsic self-calibration system is sensitive to motion. With sufficient rotational motion, all intrinsic parameters, except the composite accelerometer bias ($\mathbf{b}_a^+$), are observable, including gyroscope biases ($\mathbf{b}_{g_1}, \mathbf{b}_{g_2}$), gyroscope scale factors ($\mathbf{s}_{g_1}, \mathbf{s}_{g_2}$), and the "relative" accelerometer bias ($\mathbf{b}_a^- \triangleq \mathbf{b}_{a_1} - {}^1\mathbf{C}_2\mathbf{b}_{a_2}$), of the two IMUs. Meanwhile, certain parameters will become unobservable if the motion is specifically constrained.*

Based on this result, we have the following insight that, besides the gyroscope data, the accelerometer data of two IMUs with known extrinsics can provide extra information about angular velocity. These two sources of information fully determine the angular motion of both IMUs, and hence, the gyroscope intrinsics become solvable.

Additionally, based on (19)-(22), the accuracy of the intrinsic estimation also depends on the norm of the baseline $\left\|{}^1\mathbf{p}_2\right\|$ between the two IMUs. Under the same motion, the longer the baseline is, the better the estimation accuracy will become due to the higher signal-to-noise ratio of the system.

IV. Additional Unobservable Directions Under Degenerate Motions

In practice, the RDI platform may not consistently sustain sufficient rotational motion. Hereafter, we will further analyze the *additional* unobservable directions arising from degenerate motions. We can define these motions based on the necessary and sufficient motion condition for observability given in Theorem 1.2.

A. Constant Angular Velocity about Local X, Y, or Z Axis

When the RDI platform follows a special motion such that ${}^{I_n}\boldsymbol{\omega}(t)$ has a constant element, i.e.,

$$ {}^{I_n}\boldsymbol{\omega}(t)\cdot\mathbf{e}_i \equiv {}^{I_n}\omega_i \quad \text{for } \forall\ t,\ i=1,2 \text{ or } 3 \tag{28}$$

where ${}^{I_n}\omega_i$ denotes the constant scalar of the i-th element of ${}^{I_n}\boldsymbol{\omega}$, and $n=1,2$ for each IMU. Under this type of constraints, the matrix $\boldsymbol{\Lambda}_2$ is rank deficient if $n=2$, or $[\mathbb{K},\mathbb{L}]$ is rank deficient if $n=1$, which violates Condition (i) or (ii) in Theorem 1.2. We have the following result.

Theorem 2.1 *The RDI intrinsic self-calibration system has the following additional unobservable directions, besides the composite accelerometer bias, if condition* (28) *is satisfied:*

$$\begin{cases} \mathbf{N}_{\mathbf{b}^i_{g_1},\mathbf{s}^i_{g_1}} = \begin{bmatrix} -{}^{I_1}\omega_i\mathbf{e}_i^\top & \mathbf{0}_{1\times3} & \mathbf{e}_i^\top & \mathbf{0}_{1\times3} & \mathbf{0}_{1\times6}\end{bmatrix}^\top \text{ if } n=1 \\ \mathbf{N}_{\mathbf{b}^i_{g_2},\mathbf{s}^i_{g_2}} = \begin{bmatrix} \mathbf{0}_{1\times3} & -{}^{I_2}\omega_i\mathbf{e}_i^\top & \mathbf{0}_{1\times3} & \mathbf{e}_i^\top & \mathbf{0}_{1\times6}\end{bmatrix}^\top \text{ if } n=2 \end{cases} \tag{29}$$

PROOF See Appendix III.

Theorem 2.1 states that when the gyroscope maintains a constant local angular velocity along a specific principal axis, the bias and scale factor along this axis become ambiguous.

B. Angular Acceleration Parallel or Perpendicular to ${}^1\mathbf{p}_2$

When the RDI platform follows a special motion such that the angular acceleration ${}^{I_1}\dot{\boldsymbol{\omega}}(t)$ has a constant direction, which is parallel or perpendicular to the baseline ${}^1\mathbf{p}_2$, i.e.,

$$ {}^{I_1}\dot{\boldsymbol{\omega}} \parallel {}^1\mathbf{p}_2, \tag{30}$$

$$ \text{or} \quad {}^{I_1}\dot{\boldsymbol{\omega}} \perp {}^1\mathbf{p}_2 \ \wedge\ {}^{I_1}\dot{\boldsymbol{\omega}} \text{ dir. const.} \tag{31}$$

Under this type of constraints, the matrix $\mathbb{K}$ is rank deficient, which violates Condition (ii) in Theorem 1.2. We have the following result.

Theorem 2.2 *The RDI intrinsic self-calibration system has the following additional unobservable direction, besides the composite accelerometer bias, if condition* (30) *is satisfied:*

$$\mathbf{N}_{\mathbf{b}_g^+,\mathbf{b}_a\parallel} = \begin{bmatrix} -(\mathbf{S}_{g_1}{}^1\mathbf{p}_2)^\top & (\mathbf{S}_{g_2}{}^2\mathbf{p}_1)^\top & \mathbf{0}_{1\times6} & -(\mathbf{K}_1{}^1\mathbf{p}_2)^\top & \mathbf{0}_{1\times3}\end{bmatrix}^\top$$

PROOF See Appendix IV.

Theorem 2.3 *The RDI intrinsic self-calibration system has the following additional unobservable direction, besides the composite accelerometer bias, if condition* (31) *is satisfied:*

$$\mathbf{N}_{\mathbf{b}_g^+,\mathbf{b}_a\perp} = \begin{bmatrix} -(\mathbf{S}_{g_1}({}^{I_1}\dot{\boldsymbol{\omega}}\times{}^1\mathbf{p}_2))^\top & (\mathbf{S}_{g_2}({}^{I_2}\dot{\boldsymbol{\omega}}\times{}^2\mathbf{p}_1))^\top & \mathbf{0}_{1\times6} & -(\mathbf{K}_1({}^{I_1}\dot{\boldsymbol{\omega}}\times{}^1\mathbf{p}_2))^\top & \mathbf{0}_{1\times3}\end{bmatrix} \tag{32}$$

PROOF See Appendix V.

Herein, we have defined: ${}^{I_2}\dot{\boldsymbol{\omega}} = {}^1\mathbf{C}_2^\top\,{}^{I_1}\dot{\boldsymbol{\omega}}$ and ${}^2\mathbf{p}_1 = -{}^1\mathbf{C}_2^\top{}^1\mathbf{p}_2$. The physical interpretation of Theorem 2.2 and Theorem 2.3 is that when the gyroscope undergoes constant angular acceleration parallel or perpendicular to the baseline, the composite gyroscope bias along the baseline becomes ambiguous, as the measurements can be compensated by changing the accelerometer bias, according to (17).

TABLE I: Summary of Unobservable Intrinsics under Different Degenerate Motions

Degenerate Motion	Intrinsics with Unobservable Components
${}^{I_1}\boldsymbol{\omega}^i$ const.	$\mathbf{b}_{g_1}^i, \mathbf{s}_{g_1}^i, \mathbf{b}_a^+$
${}^{I_2}\boldsymbol{\omega}^i$ const.	$\mathbf{b}_{g_2}^i, \mathbf{s}_{g_2}^i, \mathbf{b}_a^+$
${}^{I_1}\dot{\boldsymbol{\omega}} \parallel {}^1\mathbf{p}_2$	$\mathbf{b}_{g_1}, \mathbf{b}_{g_2}, \mathbf{b}_a^+, \mathbf{b}_a^-$
${}^{I_1}\dot{\boldsymbol{\omega}} \perp {}^1\mathbf{p}_2 \wedge {}^{I_1}\dot{\boldsymbol{\omega}}$ dir. const.	$\mathbf{b}_{g_1}, \mathbf{b}_{g_2}, \mathbf{b}_a^+, \mathbf{b}_a^-$
${}^{I_1}\boldsymbol{\omega} \parallel {}^1\mathbf{p}_2$	$\mathbf{b}_{g_1}, \mathbf{b}_{g_2}, \mathbf{s}_{g_1}, \mathbf{s}_{g_2}, \mathbf{b}_a^+$
${}^{I_1}\boldsymbol{\omega} \perp {}^1\mathbf{p}_2 \ \wedge \ {}^{I_1}\boldsymbol{\omega}$ dir. const. $\wedge \ {}^{I_1}\dot{\boldsymbol{\omega}}$ const	$\mathbf{b}_{g_1}, \mathbf{b}_{g_2}, \mathbf{s}_{g_1}, \mathbf{s}_{g_2}, \mathbf{b}_a^+, \mathbf{b}_a^-$

Note: i denotes the i-th component of the vector in the x, y, z directions, $\mathbf{b}_a^+$ denotes composite accelerometer bias, and $\mathbf{b}_a^-$ denotes relative accelerometer bias. In this table, an intrinsic parameter is listed if certain components of this intrinsic parameter are unobservable, not necessarily all components, but the estimates of this intrinsic parameter may be unreliable.

C. Angular Velocity Parallel or Perpendicular to ${}^1\mathbf{p}_2$

When the RDI platform follows a special motion such that the angular velocity ${}^{I_1}\boldsymbol{\omega}(t)$ has a constant direction, which is parallel to the baseline ${}^1\mathbf{p}_2$, or is perpendicular to ${}^1\mathbf{p}_2$ with a constant angular acceleration, i.e.,

$$ {}^{I_1}\boldsymbol{\omega} \parallel {}^1\mathbf{p}_2 \tag{33} $$

$$ \text{or} \quad {}^{I_1}\boldsymbol{\omega} \perp {}^1\mathbf{p}_2 \ \wedge \ {}^{I_1}\boldsymbol{\omega} \text{ dir. const.} \ \wedge \ {}^{I_1}\dot{\boldsymbol{\omega}} \text{ const.} \tag{34} $$

Under this type of constraints, the matrix $\mathbb{K}$ and $\mathbb{L}$ are both rank deficient, which violates Condition (ii) in Theorem 1.2. We have the following result.

Theorem 2.4 *The RDI intrinsic self-calibration system has the following additional unobservable directions, besides the composite accelerometer bias, if condition* (33) *is satisfied:*

$$ \mathbf{N}_{\mathbf{b}_g^+\parallel} = \begin{bmatrix} -(\mathbf{S}_{g_1}{}^1\mathbf{p}_2)^\top & (\mathbf{S}_{g_2}{}^2\mathbf{p}_1)^\top & \mathbf{0}_{1\times 12} \end{bmatrix}^\top \tag{35} $$

$$ \mathbf{N}_{|\mathbf{s}_g|} = \begin{bmatrix} \mathbf{0}_{1\times 6} & \mathbf{s}_{g_1}^\top & \mathbf{s}_{g_2}^\top & \mathbf{0}_{1\times 6} \end{bmatrix}^\top \tag{36} $$

PROOF See Appendix VI.

Theorem 2.5 *The RDI intrinsic self-calibration system has the following additional unobservable directions, besides the composite accelerometer bias, if condition* (34) *is satisfied:*

$$ \mathbf{N}_{\mathbf{b}_g^+\perp} = \begin{bmatrix} -(\mathbf{S}_{g_1}({}^{I_1}\dot{\boldsymbol{\omega}} \times {}^1\mathbf{p}_2))^\top & (\mathbf{S}_{g_2}({}^{I_2}\dot{\boldsymbol{\omega}} \times {}^2\mathbf{p}_1))^\top & \mathbf{0}_{1\times 12} \end{bmatrix}^\top \tag{37} $$

$$ \begin{aligned} \mathbf{N}_{\mathbf{s}_g^+,\mathbf{b}_a\perp} = \Big[& \mathbf{0}_{1\times 6} \quad -(\mathbf{S}_{g_1}\boldsymbol{\Lambda}({}^{I_1}\dot{\boldsymbol{\omega}})^{-1}({}^{I_1}\dot{\boldsymbol{\omega}} \times {}^1\mathbf{p}_2))^\top \\ & (\mathbf{S}_{g_2}\boldsymbol{\Lambda}({}^{I_2}\dot{\boldsymbol{\omega}})^{-1}({}^{I_2}\dot{\boldsymbol{\omega}} \times {}^2\mathbf{p}_1))^\top \quad -(\mathbf{L}_1\boldsymbol{\Lambda}({}^{I_1}\dot{\boldsymbol{\omega}})^{-1}({}^{I_1}\dot{\boldsymbol{\omega}} \times {}^1\mathbf{p}_2))^\top \quad \mathbf{0}_{1\times 3} \Big]^\top \end{aligned} \tag{38} $$

PROOF See Appendix VII.

The unobservable direction $\mathbf{N}_{\mathbf{b}_g^+\parallel}$ and $\mathbf{N}_{\mathbf{b}_g^+\perp}$ in Theorem 2.4 and Theorem 2.5 is a special case of $\mathbf{N}_{\mathbf{b}_g^+,\mathbf{b}_a\parallel}$and $\mathbf{N}_{\mathbf{b}_g^+,\mathbf{b}_a\perp}$ in Theorem 2.2 and Theorem 2.3. Additionally, Theorem 2.4 reveals an extra unobservable direction $\mathbf{N}_{|\mathbf{s}_g|}$, corresponding to the two gyroscopes' global scale $\left\|[\mathbf{s}_{g_1}^\top \ \mathbf{s}_{g_2}^\top]\right\|$, while the relative gyroscope scale factors $\mathbf{s}_{g_1}/\left\|[\mathbf{s}_{g_1}^\top \ \mathbf{s}_{g_2}^\top]\right\|$ and $\mathbf{s}_{g_2}/\left\|[\mathbf{s}_{g_1}^\top \ \mathbf{s}_{g_2}^\top]\right\|$ remain observable. And Theorem 2.5 reveals an extra unobservable direction $\mathbf{N}_{\mathbf{s}_g^+,\mathbf{b}_a\perp}$, indicating the composite gyroscope scale factors and accelerometer bias become indistinguishable.

In summary, intrinsic self-calibration results of the RDI system are sensitive to sensor motion, specifically angular velocity and angular acceleration, and the unobservable intrinsics are summarized in Table I. Certain motions can meet one or multiple degenerate conditions simultaneously, leading to several unobservable directions and hence unreliable estimates of the intrinsics. In practice, our findings provide guidelines for improving system observability. For example, in the sensor placement of planar robots, neither the principal axes of the IMUs nor the baseline between the two IMUs should be parallel to the plane. Additionally, for online calibration of wearable IMU sensors, the rotational velocity must vary over time and rotate around axes that are neither parallel nor perpendicular to the baseline between IMUs.

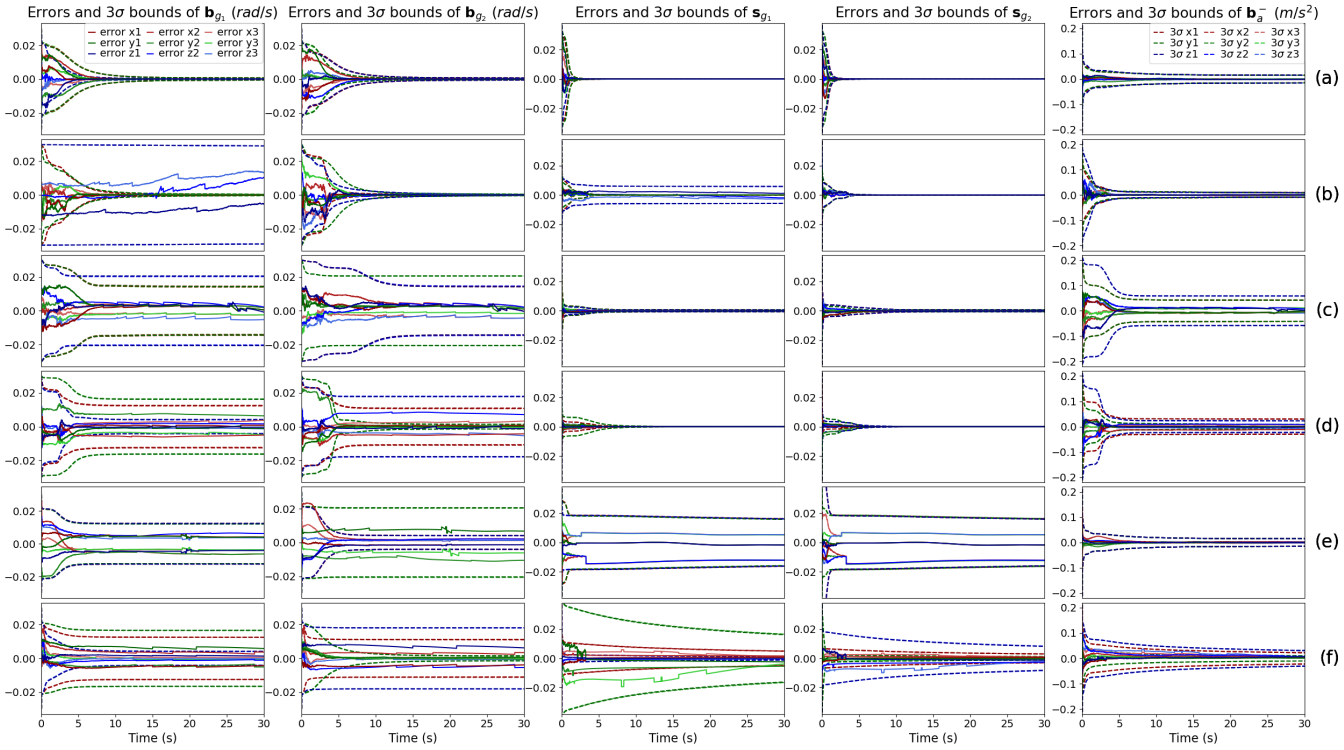

Fig. 2: Errors and 3σ bounds of intrinsic parameters for different motion patterns, based on three Monte Carlo experiments (red: x direction, green: y direction, blue: z direction; solid lines: errors, dashed lines: 3σ bounds; different color shades represent the three experiments). Each row of this figure represents a different motion pattern. Specifically, (a) corresponds to sufficient motion that satisfies the condition in Theorem 1.2. (b), (c), (d), (e) and (f) correspond to the motions constrained by the conditions in Theorem 2.1, 2.2, 2.3, 2.4, and 2.5, respectively.

V. Numerical Simulation

To verify the effectiveness of our RDI intrinsic self-calibration system under sufficient motion, and the impact of unobservable directions on the calibration results under degenerate motions, we implement an optimization-based estimator [37] for this system, and conduct Monte Carlo simulations.

We assume that the relative translation of I_2 with respect to I_1 is $[0.1, 0.1, -0.1]^\top$ meters, and the relative rotation angle axis is $-\frac{\pi}{3}[\frac{\sqrt{3}}{3}, \frac{\sqrt{3}}{3}, \frac{\sqrt{3}}{3}]^\top$. Then, we generate 30 seconds of motion data corresponding to the sufficient motion described in Theorem 1.2 and the degenerate motions described in Theorem 2.1-2.5. We conduct Monte Carlo simulations with varying measurement noise realizations and initial calibration perturbations. We select three runs for each motion, and the corresponding calibration result errors and 3σ bounds are shown in Fig. 2, which include the two IMUs' gyroscope biases and scale factors, and relative accelerometer biases for each motion. As the composite accelerometer bias is always unobservable and its error is diverged, it is omitted here. Under sufficient motion, all errors converge to zero, and the 3σ bounds continuously shrink [see Fig. 2(a)]. In contrast, the results of degenerate motions [see Fig. 2(b)-(f)] exhibit certain errors and 3σ bounds that do not converge, remaining at significant values. Specifically, in Fig. 2(b), the z-axis components of $\mathbf{b}_{g_1}$ and $\mathbf{s}_{g_1}$ do not converge. In Fig. 2(c) and 2(d), $\mathbf{b}_{g_1}$, $\mathbf{b}_{g_2}$ and $\mathbf{b}_a^-$ fail to converge. Similarly, $\mathbf{b}_{g_1}$, $\mathbf{b}_{g_2}$, $\mathbf{s}_{g_1}$, $\mathbf{s}_{g_2}$ in Fig.2(e) and $\mathbf{b}_{g_1}$, $\mathbf{b}_{g_2}$, $\mathbf{s}_{g_1}$, $\mathbf{s}_{g_2}$, $\mathbf{b}_a^-$ in Fig.2(f) fail to converge. These results are consistent with those in Table I. Note that a single unobservable direction can result in multiple parameters failing to converge. For example, in the case shown in Fig. 2(c), $\mathbf{N}_{\mathbf{b}_g^+, \mathbf{b}_a \|}$ is the only unobservable direction (aside from $\mathbf{N}_{\mathbf{b}_a^+}$), yet $\mathbf{b}_{g_1}$, $\mathbf{b}_{g_2}$ and $\mathbf{b}_a^-$ do not converge. Similarly, in Fig. 2(f), despite having only two unobservable directions $\mathbf{N}_{\mathbf{b}_g^+ \perp}$ and $\mathbf{N}_{\mathbf{s}_g^+, \mathbf{b}_a \perp}$ (aside from $\mathbf{N}_{\mathbf{b}_a^+}$), all parameters fail to converge.

The simulation results confirm that under sufficient motion, all estimated parameters, except $\mathbf{b}_a^+$, are well estimated. However, under degenerate motions, certain parameters fail to converge because of the presence of additional unobservable directions. All these results verify our observability analysis for the RDI self-calibration system.

VI. Experimental Results

In this section, we design experiments to showcase the RDI self-calibration system's performance in real-world scenarios. In our experiment, see Fig. 3, we rigidly connect two consumer-grade MEMS-IMUs to a base, aligning them with no relative rotation and a 15 cm relative translation only along the x-axis. The accurate extrinsic parameters between the two IMUs are calibrated with the aid of a stereo camera mounted on the same base. The ground truth of gyroscope scale factors of both

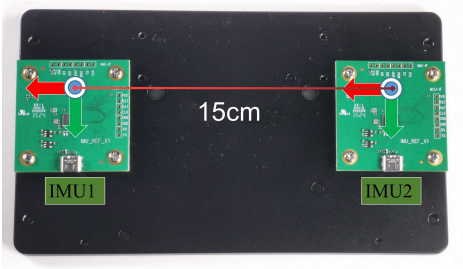

Fig. 3: Experimental setup of two MEMS-IMUs rigidly connected on a base, aligned with no rotation and a 15 cm translation along the x-axis.

TABLE II: Estimation Errors of Gyroscope Biases and Scale Factors with Randomly Assigned Values

	x	y	z
$\mathbf{b}_{g_1}$ Error (mrad/s)	0.80 ± 0.41	0.28 ± 0.13	0.94 ± 0.25
$\mathbf{b}_{g_2}$ Error (mrad/s)	0.83 ± 0.33	0.64 ± 0.21	1.10 ± 0.23
$\mathbf{s}_1$ Error (%)	-0.04 ± 0.02	-0.03 ± 0.01	-0.04 ± 0.02
$\mathbf{s}_2$ Error (%)	-0.03 ± 0.03	-0.03 ± 0.01	0.01 ± 0.02

Means and ranges of the final estimation errors for RDI self-calibration system based on 50 Monte Carlo experiments. In each run, the impact of original intrinsic parameters for both IMUs are removed, and additional random gyroscope biases and scale factors, uniformly sampled from ranges [-0.05 rad/s, 0.05 rad/s] and [-10%,10%], are introduced, respectively.

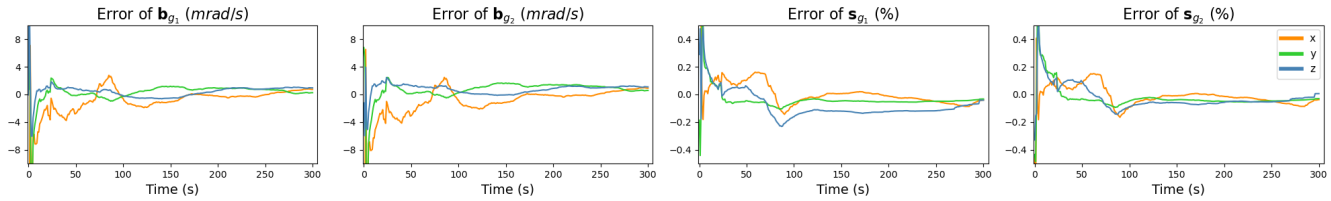

Fig. 4: Errors of gyroscope biases and scale factors over time. Initially, all errors exhibit oscillations. Subsequently, the errors of gyroscope scale factors of each IMU quickly converge to a small value (0.2%). Meanwhile, the errors of gyroscope biases rapidly converge to a small value (around 4 mrad/s), and then gradually to a even smaller value (around 1 mrad/s).

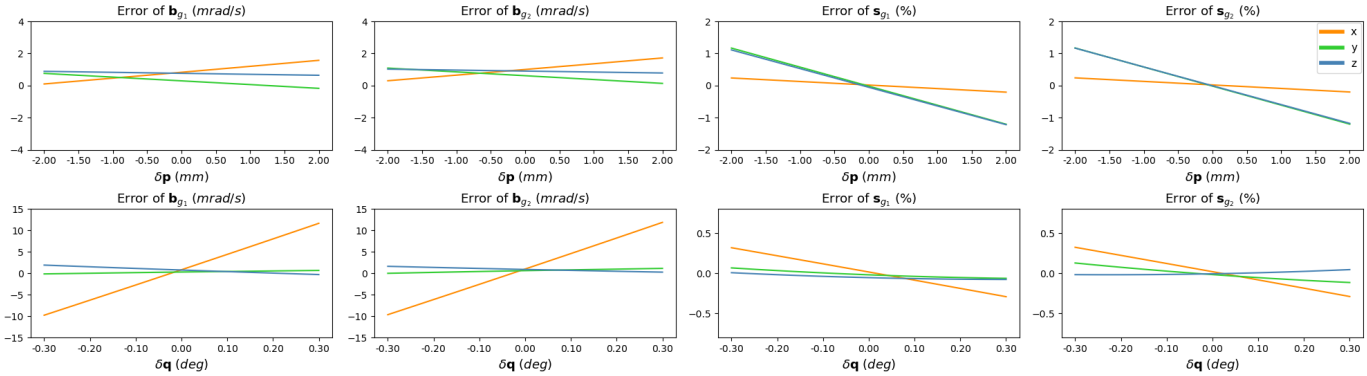

Fig. 5: Gyroscope intrinsic errors from baseline-aligned extrinsic translation (first row) and orientation (second row) perturbations. Translation perturbations along the baseline direction cause significant errors in the gyroscope scale factors perpendicular to the baseline (y, z axes), while having minimal impact on other parameters. In contrast, orientation perturbations significantly increase the gyroscope biases and scale factors errors parallel to the baseline (x axes), while having minimal impact on errors in other directions.

IMUs is calibrated using IMU-TK [25], while the ground truth of the gyroscope biases is determined by keeping the IMUs stationary for a period before and after the experiment. During the experiment, the two IMUs undergo diverse motions. Our calibration method is based on optimization framework [37].

As shown in Fig. 4, initially, all errors of gyroscope biases and scale factors of both IMUs exhibit oscillations due to insufficient motion. Subsequently, with more varied motion, these errors quickly converge to a small value. These results are consistent with Remark 1.2, demonstrating that under sufficient motion, both gyroscope biases and scale factors of the two IMUs are observable.

Building on the previous results, we extend our evaluation by introducing random gyroscope biases and scale factors into the same data. As shown in Table II, even with a wide range of intrinsic parameter distributions and large deviations from the initial values, the estimation errors remain small, indicating that our calibration system is robust to initial values. In addition, Fig. 5 shows our calibration system's performance when there are perturbations in the extrinsic parameters between two IMUs along the baseline direction. Translation variations introduce errors in gyroscope scale factors perpendicular to the baseline, with minimal impact on other parameters. Rotation variations primarily affect the gyroscope bias and scale factors parallel to the baseline, while having little effect on the perpendicular axes. These effects exhibit a linear relationship with the magnitude of the perturbations.

To summarize, the experimental results align well with our observability analysis in Section III, validating both the effectiveness and accuracy of our RDI self-calibration system. Moreover, we have demonstrated that our system remains robust to variations in initial values.

VII. Conclusions and Future Work

In this paper, we addressed the problem of infield self-calibration of intrinsics of a rigid dual-IMU system with known extrinsics. We first derived the dynamic and measurement models of this system using only IMU data and inter-IMU extrinsic constraints, which turned out to be gravity-independent. We then performed an observability analysis for this system and established a necessary and sufficient condition for the rank of the observability matrix, which depends on the angular velocity and acceleration of the platform. Then we proved that, by using both gyroscope and accelerometer data, the gyroscope biases, gyroscope scale factors, and relative accelerometer bias of the two IMUs are observable, under sufficient rotational motion. Meanwhile, the composite accelerometer bias is always unobservable. Furthermore, we determined several degenerate motions based on the motion condition, and identified the additional unobservable directions for each case. Our findings could provide guidelines for improving system observability in practice. Through numerical simulations and real-world experiments, we verified the impact of these unobservable directions on the estimation results, and our proposed RDI intrinsic self-calibration system achieved high accuracy and robustness to initial state errors on real-world data.

As part of our future work, we plan to extend our study to include more intrinsic (e.g. axis misalignments) and unknown extrinsic parameters.

Appendix I
Equivalent Matrix of Observability Matrix

In this section, we present the equivalent matrix of $\mathbf{M}$. From (23), the observability matrix $\mathbf{M}$ has the following form:

$$\mathbf{M} = \begin{bmatrix} \mathbf{M}_1 \\ \mathbf{M}_2 \\ \vdots \\ \mathbf{M}_k \\ \vdots \end{bmatrix} = \begin{bmatrix} -\mathbf{S}_{g_1}^{-1} & {}^1\mathbf{C}_2\mathbf{S}_{g_2}^{-1} & -\mathbf{\Lambda}({}^{I_1}\hat{\boldsymbol{\omega}}_1)\mathbf{S}_{g_1}^{-1} & {}^1\mathbf{C}_2\mathbf{\Lambda}({}^{I_2}\hat{\boldsymbol{\omega}}_1)\mathbf{S}_{g_2}^{-1} & \mathbf{0}_3 & \mathbf{0}_3 \\ -\mathbf{K}_1\mathbf{S}_{g_1}^{-1} & \mathbf{0}_3 & -\mathbf{L}_1\mathbf{S}_{g_1}^{-1} & \mathbf{0}_3 & \mathbf{I}_3 & -{}^1\mathbf{C}_2 \\ -\mathbf{S}_{g_1}^{-1} & {}^1\mathbf{C}_2\mathbf{S}_{g_2}^{-1} & -\mathbf{\Lambda}({}^{I_1}\hat{\boldsymbol{\omega}}_2)\mathbf{S}_{g_1}^{-1} & {}^1\mathbf{C}_2\mathbf{\Lambda}({}^{I_2}\hat{\boldsymbol{\omega}}_2)\mathbf{S}_{g_2}^{-1} & \mathbf{0}_3 & \mathbf{0}_3 \\ -\mathbf{K}_2\mathbf{S}_{g_1}^{-1} & \mathbf{0}_3 & -\mathbf{L}_2\mathbf{S}_{g_1}^{-1} & \mathbf{0}_3 & \mathbf{I}_3 & -{}^1\mathbf{C}_2 \\ \vdots & \vdots & \vdots & \vdots & \vdots & \vdots \\ -\mathbf{S}_{g_1}^{-1} & {}^1\mathbf{C}_2\mathbf{S}_{g_2}^{-1} & -\mathbf{\Lambda}({}^{I_1}\hat{\boldsymbol{\omega}}_k)\mathbf{S}_{g_1}^{-1} & {}^1\mathbf{C}_2\mathbf{\Lambda}({}^{I_2}\hat{\boldsymbol{\omega}}_k)\mathbf{S}_{g_2}^{-1} & \mathbf{0}_3 & \mathbf{0}_3 \\ -\mathbf{K}_k\mathbf{S}_{g_1}^{-1} & \mathbf{0}_3 & -\mathbf{L}_k\mathbf{S}_{g_1}^{-1} & \mathbf{0}_3 & \mathbf{I}_3 & -{}^1\mathbf{C}_2 \\ \vdots & \vdots & \vdots & \vdots & \vdots & \vdots \end{bmatrix} \tag{39}$$

To analyze the rank of the matrix $\mathbf{M}$, we apply transformations by multiplying it from the left by $\mathbf{E}_l$ and from the right by $\mathbf{E}_r$, where both $\mathbf{E}_l$ and $\mathbf{E}_r$ are invertible matrices. This process corresponds to Gaussian elimination and column permutation, resulting in the equivalent matrix $\mathbf{M}'$:

$$\mathbf{M}' = \mathbf{E}_l \cdot \mathbf{M} \cdot \mathbf{E}_r \tag{40}$$

which has a block upper-triangular form:

$$\mathbf{M}' = \begin{bmatrix} {}^1\mathbf{C}_2 & \mathbf{0}_3 & \mathbf{0}_3 & \mathbf{0}_3 & \mathbf{0}_3 & \mathbf{0}_3 \\ \mathbf{0}_3 & \mathbf{\Lambda}_2 & \mathbf{0}_3 & \mathbf{0}_3 & \mathbf{\Lambda}_1 & \mathbf{0}_3 \\ \mathbf{0}_3 & \mathbf{0}_3 & \mathbf{I}_3 & \mathbf{0}_3 & \mathbf{0}_3 & \mathbf{0}_3 \\ \mathbf{0}_3 & \mathbf{0}_3 & \mathbf{0}_3 & \mathbb{K} & \mathbb{L} & \mathbf{0}_3 \end{bmatrix} \tag{41}$$

where $\mathbf{E}_l$ and $\mathbf{E}_r$ are given by:

$$\mathbf{E}_l = \begin{bmatrix} \mathbf{I} & \mathbf{0} & \mathbf{0} & \mathbf{0} & \cdots & \mathbf{0} & \mathbf{0} & \mathbf{0} \\ -\mathbf{I} & \mathbf{0} & \mathbf{I} & \mathbf{0} & \cdots & \mathbf{0} & \mathbf{0} & \mathbf{0} \\ \vdots & \vdots & \vdots & \vdots & \vdots & \vdots & \vdots & \vdots \\ -\mathbf{I} & \mathbf{0} & \mathbf{0} & \mathbf{0} & \cdots & \mathbf{0} & \mathbf{I} & \mathbf{0} \\ \mathbf{0} & \mathbf{I} & \mathbf{0} & \mathbf{0} & \cdots & \mathbf{0} & \mathbf{0} & \mathbf{0} \\ \mathbf{0} & -\mathbf{I} & \mathbf{0} & \mathbf{I} & \cdots & \mathbf{0} & \mathbf{0} & \mathbf{0} \\ \vdots & \vdots & \vdots & \vdots & \vdots & \vdots & \vdots & \vdots \\ \mathbf{0} & -\mathbf{I} & \mathbf{0} & \mathbf{0} & \cdots & \mathbf{0} & \mathbf{0} & \mathbf{I} \end{bmatrix}, \mathbf{E}_r = \begin{bmatrix} \mathbf{0} & \mathbf{0} & \mathbf{0} & -\mathbf{S}_{g_1} & \mathbf{0} & \mathbf{0} \\ \mathbf{S}_{g_2} & -\mathbf{S}_{g_2}\mathbf{\Lambda}({}^{I_2}\hat{\boldsymbol{\omega}}_1) & \mathbf{0} & -\mathbf{S}_{g_2}{}^1\mathbf{C}_2^\top & -\mathbf{S}_{g_2}{}^1\mathbf{C}_2^\top\mathbf{\Lambda}({}^{I_1}\hat{\boldsymbol{\omega}}_1) & \mathbf{0} \\ \mathbf{0} & \mathbf{0} & \mathbf{0} & \mathbf{0} & -\mathbf{S}_{g_1} & \mathbf{0} \\ \mathbf{0} & \mathbf{S}_{g_2} & \mathbf{0} & \mathbf{0} & \mathbf{0} & \mathbf{0} \\ \mathbf{0} & \mathbf{0} & \mathbf{I} & -\mathbf{K}_1 & -\mathbf{L}_1 & \mathbf{0} \\ \mathbf{0} & \mathbf{0} & \mathbf{0} & \mathbf{0} & \mathbf{0} & \mathbf{I} \end{bmatrix} \tag{42}$$

Appendix II
Observability under Sufficient Motion

In this section, we present an example of sufficient motion, and prove that Condition (i)and (ii) is satisfied under such motion. Before proving this, we state the following lemma.

Lemma 1 *Given two nonzero vectors* $\mathbf{a}$ *and* $\mathbf{b}$*, the matrix* $\mathbf{J} = [\mathbf{b} \times \mathbf{a}]_\times + [\mathbf{b}\times][\mathbf{a}\times]$ *is not full rank if and only if either* $\mathbf{b} \parallel \mathbf{a}$ *or* $\mathbf{b} \perp \mathbf{a}$*.*

PROOF (LEMMA 1) Without loss of generality, assume $\mathbf{a} = [1,0,0]^\top$ and $\mathbf{b} = [x,y,z]^\top$. The matrix $\mathbf{J}$ takes the form:

$$\mathbf{J} = \begin{bmatrix} 0 & 2y & 2z \\ -y & -x & 0 \\ -z & 0 & -x \end{bmatrix} \tag{43}$$

Its determinant is:

$$\det(\mathbf{J}) = -2x(y^2 + z^2) \tag{44}$$

It's obvious that when the determinant vanishes:

$$\det(\mathbf{J}) = 0 \Leftrightarrow (\mathbf{b} \parallel \mathbf{a}) \vee (\mathbf{b} \perp \mathbf{a}) \tag{45}$$

Further, we can derive the right nullspace of $\mathbf{J}$:

$$null(\mathbf{J}) = \begin{cases} \mathbf{a} & \text{if } \mathbf{a} \parallel \mathbf{b} \\ \mathbf{b} \times \mathbf{a} & \text{if } \mathbf{a} \perp \mathbf{b} \end{cases} \tag{46}$$

■

Hereafter, we give an example of sufficient motion, which is defined as:

$$\begin{cases} \vdots \\ {}^{I_2}\boldsymbol{\omega}_1 = \alpha_1 \mathbf{u}, \\ {}^{I_2}\boldsymbol{\omega}_2 = \alpha_2 \mathbf{u}, \\ \vdots \end{cases} \quad \text{and} \quad \begin{cases} \vdots \\ {}^{I_1}\boldsymbol{\omega}_1 = \beta_1 \mathbf{v}, \ {}^{I_1}\dot{\boldsymbol{\omega}}_1 = \mathbf{v} \\ {}^{I_1}\boldsymbol{\omega}_2 = \beta_2 \mathbf{v}, \ {}^{I_1}\dot{\boldsymbol{\omega}}_2 = \mathbf{v} \\ {}^{I_1}\boldsymbol{\omega}_3 = \beta_3 \mathbf{v}, \ {}^{I_1}\dot{\boldsymbol{\omega}}_3 = \mathbf{v} \\ \vdots \end{cases} \tag{47}$$

$$\begin{aligned} &\text{with} \quad \alpha_1 \neq \alpha_2, \quad \beta_1 \neq \beta_2 \neq \beta_3, \\ &\text{and} \quad \mathbf{v} \nparallel {}^1\mathbf{p}_2, \ \mathbf{v} \not\perp {}^1\mathbf{p}_2, \quad \mathbf{u}_x, \mathbf{u}_y, \mathbf{u}_z, \mathbf{v}_x, \mathbf{v}_y, \mathbf{v}_z \neq 0, \end{aligned} \tag{48}$$

This motion corresponds to a simple case where the platform rotates around a single axis, which is not parallel or perpendicular to the baseline ${}^1\mathbf{p}_2$, with time-varying rotational velocity. From (21) (22) and (27) we have:

$$\boldsymbol{\Lambda}_2 = \begin{bmatrix} \vdots \\ {}^1\mathbf{C}_2 \boldsymbol{\Lambda}\left((\alpha_2 - \alpha_1)\mathbf{u}\right) \\ \vdots \end{bmatrix}, [\mathbb{K}, \mathbb{L}] = \begin{bmatrix} \vdots & \vdots \\ (\beta_2 - \beta_1)\,\mathbf{K}_v & (\beta_2 - \beta_1)^2\,\mathbf{K}_v \boldsymbol{\Lambda}(\mathbf{v}) \\ (\beta_3 - \beta_1)\,\mathbf{K}_v & (\beta_3 - \beta_1)^2\,\mathbf{K}_v \boldsymbol{\Lambda}(\mathbf{v}) \\ \vdots & \vdots \end{bmatrix} \tag{49}$$

where $\mathbf{K}_v = \lfloor \mathbf{v} \times {}^1\mathbf{p}_2 \rfloor + \lfloor \mathbf{v} \rfloor \lfloor {}^1\mathbf{p}_2 \rfloor$. $\boldsymbol{\Lambda}_2$ is obviously full rank as $\alpha_1 \neq \alpha_2$ and $\mathbf{u}_x, \mathbf{u}_y, \mathbf{u}_z \neq 0$ [see (48)]. As for the matrix $[\mathbb{K}, \mathbb{L}]$, we can obtain an equivalent matrix through row transformation as follows:

$$[\mathbb{K}, \mathbb{L}]' = \begin{bmatrix} \vdots & \vdots \\ (\beta_2 - \beta_1)\mathbf{K}_v & (\beta_2 - \beta_1)^2 \mathbf{K}_v \boldsymbol{\Lambda}(\mathbf{v}) \\ 0 & (\beta_3 - \beta_1)(\beta_3 - \beta_2)\mathbf{K}_v \boldsymbol{\Lambda}(\mathbf{v}) \\ \vdots & \vdots \end{bmatrix} \tag{50}$$

According to Lemma 1, as $\beta_1 \neq \beta_2 \neq \beta_3$, $\mathbf{v} \nparallel {}^1\mathbf{p}_2, \mathbf{v} \not\perp {}^1\mathbf{p}_2$ in (48), $\mathbf{K}_v$ has full rank. Additionally, as $\mathbf{v}_x, \mathbf{v}_y, \mathbf{v}_z \neq 0$, $\boldsymbol{\Lambda}(\mathbf{v})$ has full rank. Hence, the matrix $[\mathbb{K}, \mathbb{L}]'$ and its equivalent matrix $[\mathbb{K}, \mathbb{L}]$ have full rank.

Therefore, the motion defined in (47)-(48) is a sufficient motion that meets Condition (i) and (ii).

APPENDIX III
PROOF OF THEOREM 2.1

In what follows, we verify the unobservable directions $\mathbf{N}_{\mathbf{b}^i_{g_1}, \mathbf{s}^i_{g_1}}$ and $\mathbf{N}_{\mathbf{b}^i_{g_2}, \mathbf{s}^i_{g_2}}$ of the RDI system when the condition (28) is satisfied.

A. Verification of Unobservable Direction $\mathbf{N}_{\mathbf{b}_{g_1}^i,\mathbf{s}_{g_1}^i}$

$$\mathbf{M}_k\mathbf{N}_{\mathbf{b}_{g_1}^i,\mathbf{s}_{g_1}^i} = \begin{bmatrix} -\mathbf{S}_{g_1}^{-1} & {}^1\mathbf{C}_2\mathbf{S}_{g_2}^{-1} & -\mathbf{\Lambda}({}^{I_1}\boldsymbol{\omega}_k)\mathbf{S}_{g_1}^{-1} & {}^1\mathbf{C}_2\mathbf{\Lambda}({}^{I_2}\boldsymbol{\omega}_k)\mathbf{S}_{g_2}^{-1} & \mathbf{0}_3 & \mathbf{0}_3 \\ -\mathbf{K}_k\mathbf{S}_{g_1}^{-1} & \mathbf{0}_3 & -\mathbf{L}_k\mathbf{S}_{g_1}^{-1} & \mathbf{0}_3 & \mathbf{I}_3 & -{}^1\mathbf{C}_2 \end{bmatrix} \begin{bmatrix} -{}^{I_1}\omega_i\mathbf{e}_i \\ \mathbf{0}_{3\times1} \\ \mathbf{e}_i \\ \mathbf{0}_{9\times1} \end{bmatrix} \tag{51}$$

$$= \begin{bmatrix} \mathbf{S}_{g_1}^{-1\,I_1}\omega_i\mathbf{e}_i - \mathbf{\Lambda}({}^{I_1}\boldsymbol{\omega}_k)\mathbf{S}_{g_1}^{-1}\mathbf{e}_i \\ \mathbf{K}_k\mathbf{S}_{g_1}^{-1\,I_1}\omega_i\mathbf{e}_i - \mathbf{L}_k\mathbf{S}_{g_1}^{-1}\mathbf{e}_i \end{bmatrix} \tag{52}$$

$$= \begin{bmatrix} \mathbf{S}_{g_1}^{-1\,I_1}\omega_i\mathbf{e}_i - \mathbf{S}_{g_1}^{-1}\mathbf{\Lambda}({}^{I_1}\boldsymbol{\omega}_k)\mathbf{e}_i \\ \mathbf{K}_k\mathbf{S}_{g_1}^{-1\,I_1}\omega_i\mathbf{e}_i - (\mathbf{K}_k\mathbf{\Lambda}({}^{I_1}\hat{\boldsymbol{\omega}}_k) + \lfloor{}^1\mathbf{p}_2\rfloor\mathbf{\Lambda}({}^{I_1}\dot{\hat{\boldsymbol{\omega}}}_k))\mathbf{S}_{g_1}^{-1}\mathbf{e}_i \end{bmatrix} \tag{53}$$

$$= \begin{bmatrix} \mathbf{S}_{g_1}^{-1\,I_1}\omega_i\mathbf{e}_i - \mathbf{S}_{g_1}^{-1\,I_1}\omega_i\mathbf{e}_i \\ \mathbf{K}_k\mathbf{S}_{g_1}^{-1\,I_1}\omega_i\mathbf{e}_i - (\mathbf{K}_k\mathbf{S}_{g_1}^{-1\,I_1}\mathbf{\Lambda}({}^{I_1}\hat{\boldsymbol{\omega}}_k)\mathbf{e}_i + \lfloor{}^1\mathbf{p}_2\rfloor\mathbf{S}_{g_1}^{-1}\mathbf{\Lambda}({}^{I_1}\dot{\hat{\boldsymbol{\omega}}}_k)\mathbf{e}_i) \end{bmatrix} \tag{54}$$

$$= \begin{bmatrix} \mathbf{0}_{3\times1} \\ \mathbf{K}_k\mathbf{S}_{g_1}^{-1\,I_1}\omega_i\mathbf{e}_i - (\mathbf{K}_k\mathbf{S}_{g_1}^{-1\,I_1}\omega_i\mathbf{e}_i + \mathbf{0}_{3\times1}) \end{bmatrix} \tag{55}$$

$$= \mathbf{0}_{6\times1} \tag{56}$$

where the equality from (52) to (55) follows from equation (22) and the motion condition given in equation (28).

B. Verification of Unobservable Direction $\mathbf{N}_{\mathbf{b}_{g_2}^i,\mathbf{s}_{g_2}^i}$

$$\mathbf{M}_k\mathbf{N}_{\mathbf{b}_{g_2}^i,\mathbf{s}_{g_2}^i} = \begin{bmatrix} -\mathbf{S}_{g_1}^{-1} & {}^1\mathbf{C}_2\mathbf{S}_{g_2}^{-1} & -\mathbf{\Lambda}({}^{I_1}\boldsymbol{\omega}_k)\mathbf{S}_{g_1}^{-1} & {}^1\mathbf{C}_2\mathbf{\Lambda}({}^{I_2}\boldsymbol{\omega}_k)\mathbf{S}_{g_2}^{-1} & \mathbf{0}_3 & \mathbf{0}_3 \\ -\mathbf{K}_k\mathbf{S}_{g_1}^{-1} & \mathbf{0}_3 & -\mathbf{L}_k\mathbf{S}_{g_1}^{-1} & \mathbf{0}_3 & \mathbf{I}_3 & -{}^1\mathbf{C}_2 \end{bmatrix} \begin{bmatrix} \mathbf{0}_{3\times1} \\ -{}^{I_2}\omega_i\mathbf{e}_i \\ \mathbf{0}_{3\times1} \\ \mathbf{e}_i \\ \mathbf{0}_{6\times1} \end{bmatrix} \tag{57}$$

$$= \begin{bmatrix} -{}^1\mathbf{C}_2\mathbf{S}_{g_2}^{-1\,I_2}\omega_i\mathbf{e}_i + {}^1\mathbf{C}_2\mathbf{\Lambda}({}^{I_2}\boldsymbol{\omega}_k)\mathbf{S}_{g_2}^{-1}\mathbf{e}_i \\ \mathbf{0}_{3\times1} \end{bmatrix} \tag{58}$$

$$= \begin{bmatrix} -{}^1\mathbf{C}_2\mathbf{S}_{g_2}^{-1\,I_2}\omega_i\mathbf{e}_i + {}^1\mathbf{C}_2\mathbf{S}_{g_2}^{-1}\mathbf{\Lambda}({}^{I_2}\boldsymbol{\omega}_k)\mathbf{e}_i \\ \mathbf{0}_{3\times1} \end{bmatrix} \tag{59}$$

$$= \begin{bmatrix} -{}^1\mathbf{C}_2\mathbf{S}_{g_2}^{-1\,I_2}\omega_i\mathbf{e}_i + {}^1\mathbf{C}_2\mathbf{S}_{g_2}^{-1\,I_2}\omega_i\mathbf{e}_i \\ \mathbf{0}_{3\times1} \end{bmatrix} \tag{60}$$

$$= \mathbf{0}_{6\times1} \tag{61}$$

where the equality from (58) to (60) follows from the motion condition given in equation (28).

APPENDIX IV
PROOF OF THEOREM 2.2

In what follows, we verify the unobservable direction $\mathbf{N}_{\mathbf{b}_g^+,\mathbf{b}_a\|}$ of the RDI system when the condition (30) is satisfied.

$$\mathbf{M}_k\mathbf{N}_{\mathbf{b}_g^+,\mathbf{b}_a\|} = \begin{bmatrix} -\mathbf{S}_{g_1}^{-1} & {}^1\mathbf{C}_2\mathbf{S}_{g_2}^{-1} & -\mathbf{\Lambda}({}^{I_1}\boldsymbol{\omega}_k)\mathbf{S}_{g_1}^{-1} & {}^1\mathbf{C}_2\mathbf{\Lambda}({}^{I_2}\boldsymbol{\omega}_k)\mathbf{S}_{g_2}^{-1} & \mathbf{0}_3 & \mathbf{0}_3 \\ -\mathbf{K}_k\mathbf{S}_{g_1}^{-1} & \mathbf{0}_3 & -\mathbf{L}_k\mathbf{S}_{g_1}^{-1} & \mathbf{0}_3 & \mathbf{I}_3 & -{}^1\mathbf{C}_2 \end{bmatrix} \begin{bmatrix} -\mathbf{S}_{g_1}{}^1\mathbf{p}_2 \\ \mathbf{S}_{g_2}{}^2\mathbf{p}_1 \\ \mathbf{0}_{6\times1} \\ -\mathbf{K}_1{}^1\mathbf{p}_2 \\ \mathbf{0}_{3\times1} \end{bmatrix} \tag{62}$$

$$= \begin{bmatrix} \mathbf{S}_{g_1}^{-1}\mathbf{S}_{g_1}{}^1\mathbf{p}_2 + {}^1\mathbf{C}_2\mathbf{S}_{g_2}^{-1}\mathbf{S}_{g_2}{}^2\mathbf{p}_1 \\ \mathbf{K}_k\mathbf{S}_{g_1}^{-1}\mathbf{S}_{g_1}{}^1\mathbf{p}_2 - \mathbf{K}_1{}^1\mathbf{p}_2 \end{bmatrix} \tag{63}$$

$$= \begin{bmatrix} {}^1\mathbf{p}_2 + {}^1\mathbf{C}_2{}^2\mathbf{p}_1 \\ (\mathbf{K}_k - \mathbf{K}_1){}^1\mathbf{p}_2 \end{bmatrix} \tag{64}$$

$$= \begin{bmatrix} \mathbf{0}_{3\times1} \\ \left(\lfloor({}^{I_1}\boldsymbol{\omega}_k - {}^{I_1}\boldsymbol{\omega}_1)\times{}^1\mathbf{p}_2\rfloor + \lfloor{}^{I_1}\boldsymbol{\omega}_k - {}^{I_1}\boldsymbol{\omega}_1\rfloor\lfloor{}^1\mathbf{p}_2\rfloor\right){}^1\mathbf{p}_2 \end{bmatrix} \tag{65}$$

when (30) is satisfied, there exist a scalar α such that:

$$\Leftrightarrow \mathbf{M}_k\mathbf{N}_{\mathbf{b}_g^+,\mathbf{b}_a\|} = \begin{bmatrix} \mathbf{0}_{3\times1} \\ \alpha\left(\lfloor{}^{I_1}\dot{\boldsymbol{\omega}}\times{}^1\mathbf{p}_2\rfloor + \lfloor{}^{I_1}\dot{\boldsymbol{\omega}}\rfloor\lfloor{}^1\mathbf{p}_2\rfloor\right){}^1\mathbf{p}_2 \end{bmatrix} \tag{66}$$

Additionally, from the condition (30) which states ${}^{I_1}\dot{\boldsymbol{\omega}} \parallel {}^{1}\mathbf{p}_2$, we can derive the following according to Lemma 1:

$$\Leftrightarrow \mathbf{M}_k\mathbf{N}_{\mathbf{b}_g^+,\mathbf{b}_a\parallel} = \mathbf{0}_{6\times 1} \tag{67}$$

APPENDIX V
PROOF OF THEOREM 2.3

In what follows, we verify the unobservable direction $\mathbf{N}_{\mathbf{b}_g^+,\mathbf{b}_a\perp}$ of the RDI system when the condition (31) is satisfied.

$$\mathbf{M}_k\mathbf{N}_{\mathbf{b}_g^+,\mathbf{b}_a\perp} = \begin{bmatrix} -\mathbf{S}_{g_1}^{-1} & {}^{1}\mathbf{C}_2\mathbf{S}_{g_2}^{-1} & -\boldsymbol{\Lambda}({}^{I_1}\boldsymbol{\omega}_k)\mathbf{S}_{g_1}^{-1} & {}^{1}\mathbf{C}_2\boldsymbol{\Lambda}({}^{I_2}\boldsymbol{\omega}_k)\mathbf{S}_{g_2}^{-1} & \mathbf{0}_3 & \mathbf{0}_3 \\ -\mathbf{K}_k\mathbf{S}_{g_1}^{-1} & \mathbf{0}_3 & -\mathbf{L}_k\mathbf{S}_{g_1}^{-1} & \mathbf{0}_3 & \mathbf{I}_3 & -{}^{1}\mathbf{C}_2 \end{bmatrix} \begin{bmatrix} -\mathbf{S}_{g_1}({}^{I_1}\dot{\boldsymbol{\omega}} \times {}^{1}\mathbf{p}_2) \\ \mathbf{S}_{g_2}({}^{I_2}\dot{\boldsymbol{\omega}} \times {}^{2}\mathbf{p}_1) \\ \mathbf{0}_{6\times 1} \\ -\mathbf{K}_1({}^{I_1}\dot{\boldsymbol{\omega}} \times {}^{1}\mathbf{p}_2) \\ \mathbf{0}_{3\times 1} \end{bmatrix} \tag{68}$$

$$= \begin{bmatrix} \mathbf{S}_{g_1}^{-1}\mathbf{S}_{g_1}({}^{I_1}\dot{\boldsymbol{\omega}} \times {}^{1}\mathbf{p}_2) + {}^{1}\mathbf{C}_2\mathbf{S}_{g_2}^{-1}\mathbf{S}_{g_2}({}^{I_2}\dot{\boldsymbol{\omega}} \times {}^{2}\mathbf{p}_1) \\ \mathbf{K}_k\mathbf{S}_{g_1}^{-1}\mathbf{S}_{g_1}({}^{I_1}\dot{\boldsymbol{\omega}} \times {}^{1}\mathbf{p}_2) - \mathbf{K}_1({}^{I_1}\dot{\boldsymbol{\omega}} \times {}^{1}\mathbf{p}_2) \end{bmatrix} \tag{69}$$

$$= \begin{bmatrix} ({}^{I_1}\dot{\boldsymbol{\omega}} \times {}^{1}\mathbf{p}_2) + {}^{1}\mathbf{C}_2({}^{I_2}\dot{\boldsymbol{\omega}} \times {}^{2}\mathbf{p}_1) \\ (\mathbf{K}_k - \mathbf{K}_1)({}^{I_1}\dot{\boldsymbol{\omega}} \times {}^{1}\mathbf{p}_2) \end{bmatrix} \tag{70}$$

$$= \begin{bmatrix} \mathbf{0}_{3\times 1} \\ \left(\lfloor({}^{I_1}\boldsymbol{\omega}_k - {}^{I_1}\boldsymbol{\omega}_1) \times {}^{1}\mathbf{p}_2\rfloor + \lfloor {}^{I_1}\boldsymbol{\omega}_k - {}^{I_1}\boldsymbol{\omega}_1\rfloor\lfloor {}^{1}\mathbf{p}_2\rfloor\right)({}^{I_1}\dot{\boldsymbol{\omega}} \times {}^{1}\mathbf{p}_2) \end{bmatrix} \tag{71}$$

when (31) is satisfied, there exist a scalar α such that:

$$\Leftrightarrow \mathbf{M}_k\mathbf{N}_{\mathbf{b}_g^+,\mathbf{b}_a\perp} = \begin{bmatrix} \mathbf{0}_{3\times 1} \\ \alpha\left(\lfloor {}^{I_1}\dot{\boldsymbol{\omega}} \times {}^{1}\mathbf{p}_2\rfloor + \lfloor {}^{I_1}\dot{\boldsymbol{\omega}}\rfloor\lfloor {}^{1}\mathbf{p}_2\rfloor\right)({}^{I_1}\dot{\boldsymbol{\omega}} \times {}^{1}\mathbf{p}_2) \end{bmatrix} \tag{72}$$

Additionally, from the condition (31) which states ${}^{I_1}\dot{\boldsymbol{\omega}} \perp {}^{1}\mathbf{p}_2$, we can derive the following according to Lemma 1:

$$\Leftrightarrow \mathbf{M}_k\mathbf{N}_{\mathbf{b}_g^+,\mathbf{b}_a\perp} = \mathbf{0}_{6\times 1} \tag{73}$$

APPENDIX VI
PROOF OF THEOREM 2.4

In what follows, we verify the unobservable directions $\mathbf{N}_{\mathbf{b}_g^+\parallel}$ and $\mathbf{N}_{|\mathbf{s}_g|}$ of the RDI system when the condition (33) is satisfied.

A. Verification of Unobservable Direction $\mathbf{N}_{\mathbf{b}_g^+\parallel}$

$$\mathbf{M}_k\mathbf{N}_{\mathbf{b}_g^+\parallel} = \begin{bmatrix} -\mathbf{S}_{g_1}^{-1} & {}^{1}\mathbf{C}_2\mathbf{S}_{g_2}^{-1} & -\boldsymbol{\Lambda}({}^{I_1}\boldsymbol{\omega}_k)\mathbf{S}_{g_1}^{-1} & {}^{1}\mathbf{C}_2\boldsymbol{\Lambda}({}^{I_2}\boldsymbol{\omega}_k)\mathbf{S}_{g_2}^{-1} & \mathbf{0}_3 & \mathbf{0}_3 \\ -\mathbf{K}_k\mathbf{S}_{g_1}^{-1} & \mathbf{0}_3 & -\mathbf{L}_k\mathbf{S}_{g_1}^{-1} & \mathbf{0}_3 & \mathbf{I}_3 & -{}^{1}\mathbf{C}_2 \end{bmatrix} \begin{bmatrix} -\mathbf{S}_{g_1}{}^{1}\mathbf{p}_2 \\ \mathbf{S}_{g_2}{}^{2}\mathbf{p}_1 \\ \mathbf{0}_{12\times 1} \end{bmatrix} \tag{74}$$

$$= \begin{bmatrix} \mathbf{S}_{g_1}^{-1}\mathbf{S}_{g_1}{}^{1}\mathbf{p}_2 + {}^{1}\mathbf{C}_2\mathbf{S}_{g_2}^{-1}\mathbf{S}_{g_2}{}^{2}\mathbf{p}_1 \\ \mathbf{K}_k\mathbf{S}_{g_1}^{-1}\mathbf{S}_{g_1}{}^{1}\mathbf{p}_2 \end{bmatrix} \tag{75}$$

$$= \begin{bmatrix} {}^{1}\mathbf{p}_2 + {}^{1}\mathbf{C}_2{}^{2}\mathbf{p}_1 \\ \mathbf{K}_k{}^{1}\mathbf{p}_2 \end{bmatrix} \tag{76}$$

$$= \begin{bmatrix} \mathbf{0}_{3\times 1} \\ \left(\lfloor {}^{I_1}\boldsymbol{\omega}_k \times {}^{1}\mathbf{p}_2\rfloor + \lfloor {}^{I_1}\boldsymbol{\omega}_k\rfloor\lfloor {}^{1}\mathbf{p}_2\rfloor\right){}^{1}\mathbf{p}_2 \end{bmatrix} \tag{77}$$

when (33) is satisfied, ${}^{I_1}\boldsymbol{\omega}_k \parallel {}^{1}\mathbf{p}_2$, according to Lemma 1, we have:

$$\Leftrightarrow \mathbf{M}_k\mathbf{N}_{\mathbf{b}_g^+\parallel} = \mathbf{0}_{6\times 1} \tag{78}$$

B. Verification of Unobservable Direction $\mathbf{N}_{|\mathbf{s}_g|}$

$$\mathbf{M}_k\mathbf{N}_{|\mathbf{s}_g|} = \begin{bmatrix} -\mathbf{S}_{g_1}^{-1} & {}^1\mathbf{C}_2\mathbf{S}_{g_2}^{-1} & -\mathbf{\Lambda}({}^{I_1}\boldsymbol{\omega}_k)\mathbf{S}_{g_1}^{-1} & {}^1\mathbf{C}_2\mathbf{\Lambda}({}^{I_2}\boldsymbol{\omega}_k)\mathbf{S}_{g_2}^{-1} & \mathbf{0}_3 & \mathbf{0}_3 \\ -\mathbf{K}_k\mathbf{S}_{g_1}^{-1} & \mathbf{0}_3 & -\mathbf{L}_k\mathbf{S}_{g_1}^{-1} & \mathbf{0}_3 & \mathbf{I}_3 & -{}^1\mathbf{C}_2 \end{bmatrix} \begin{bmatrix} \mathbf{0}_{6\times1} \\ \mathbf{s}_{g_1} \\ \mathbf{s}_{g_2} \\ \mathbf{0}_{6\times1} \end{bmatrix} \tag{79}$$

$$= \begin{bmatrix} -\mathbf{\Lambda}({}^{I_1}\boldsymbol{\omega}_k)\mathbf{S}_{g_1}^{-1}\mathbf{s}_{g_1} + {}^1\mathbf{C}_2\mathbf{\Lambda}({}^{I_2}\boldsymbol{\omega}_k)\mathbf{S}_{g_2}^{-1}\mathbf{s}_{g_2} \\ -\mathbf{L}_k\mathbf{S}_{g_1}^{-1}\mathbf{s}_{g_1} \end{bmatrix} \tag{80}$$

$$= \begin{bmatrix} -\mathbf{\Lambda}({}^{I_1}\boldsymbol{\omega}_k)[1\ 1\ 1]^\top + {}^1\mathbf{C}_2\mathbf{\Lambda}({}^{I_2}\boldsymbol{\omega}_k)[1\ 1\ 1]^\top \\ -\mathbf{L}_k[1\ 1\ 1]^\top \end{bmatrix} \tag{81}$$

$$= \begin{bmatrix} -{}^{I_1}\boldsymbol{\omega}_k + {}^1\mathbf{C}_2\,{}^{I_2}\boldsymbol{\omega}_k \\ -\mathbf{L}_k[1\ 1\ 1]^\top \end{bmatrix} \tag{82}$$

$$= \begin{bmatrix} \mathbf{0}_{3\times1} \\ -\mathbf{L}_k[1\ 1\ 1]^\top \end{bmatrix} \tag{83}$$

Applying (21) and (22) yields:

$$\Leftrightarrow \mathbf{M}_k\mathbf{N}_{|\mathbf{s}_g|} = \begin{bmatrix} \mathbf{0}_{3\times1} \\ -\left((\lfloor {}^{I_1}\hat{\boldsymbol{\omega}}_k \times {}^1\mathbf{p}_2\rfloor + \lfloor {}^{I_1}\hat{\boldsymbol{\omega}}_k\rfloor\lfloor {}^1\mathbf{p}_2\rfloor)\mathbf{\Lambda}({}^{I_1}\boldsymbol{\omega}_k) + \lfloor {}^1\mathbf{p}_2\rfloor\mathbf{\Lambda}({}^{I_1}\dot{\boldsymbol{\omega}}_k)\right)[1\ 1\ 1]^\top \end{bmatrix} \tag{84}$$

$$= \begin{bmatrix} \mathbf{0}_{3\times1} \\ -(\lfloor {}^{I_1}\hat{\boldsymbol{\omega}}_k \times {}^1\mathbf{p}_2\rfloor + \lfloor {}^{I_1}\hat{\boldsymbol{\omega}}_k\rfloor\lfloor {}^1\mathbf{p}_2\rfloor)\,{}^{I_1}\boldsymbol{\omega}_k + \lfloor {}^1\mathbf{p}_2\rfloor\,{}^{I_1}\dot{\boldsymbol{\omega}}_k \end{bmatrix} \tag{85}$$

when (33) is satisfied, ${}^{I_1}\boldsymbol{\omega}_k \parallel {}^1\mathbf{p}_2$ and ${}^{I_1}\dot{\boldsymbol{\omega}}_k \parallel {}^1\mathbf{p}_2$, according to Lemma 1, we have:

$$\Leftrightarrow \mathbf{M}_k\mathbf{N}_{|\mathbf{s}_g|} = \mathbf{0}_{6\times1} \tag{86}$$

Appendix VII
Proof of Theorem 2.5

In what follows, we verify the unobservable directions $\mathbf{N}_{\mathbf{b}_g^+\perp}$ and $\mathbf{N}_{\mathbf{s}_g^+,\mathbf{b}_a\perp}$ of the RDI system when the condition (34) is satisfied.

A. Verification of Unobservable Direction $\mathbf{N}_{\mathbf{b}_g^+\perp}$

$$\mathbf{M}_k\mathbf{N}_{\mathbf{b}_g^+\perp} = \begin{bmatrix} -\mathbf{S}_{g_1}^{-1} & {}^1\mathbf{C}_2\mathbf{S}_{g_2}^{-1} & -\mathbf{\Lambda}({}^{I_1}\boldsymbol{\omega}_k)\mathbf{S}_{g_1}^{-1} & {}^1\mathbf{C}_2\mathbf{\Lambda}({}^{I_2}\boldsymbol{\omega}_k)\mathbf{S}_{g_2}^{-1} & \mathbf{0}_3 & \mathbf{0}_3 \\ -\mathbf{K}_k\mathbf{S}_{g_1}^{-1} & \mathbf{0}_3 & -\mathbf{L}_k\mathbf{S}_{g_1}^{-1} & \mathbf{0}_3 & \mathbf{I}_3 & -{}^1\mathbf{C}_2 \end{bmatrix} \begin{bmatrix} -\mathbf{S}_{g_1}({}^{I_1}\dot{\boldsymbol{\omega}} \times {}^1\mathbf{p}_2) \\ \mathbf{S}_{g_2}({}^{I_2}\dot{\boldsymbol{\omega}} \times {}^2\mathbf{p}_1) \\ \mathbf{0}_{12\times1} \end{bmatrix} \tag{87}$$

$$= \begin{bmatrix} \mathbf{S}_{g_1}^{-1}\mathbf{S}_{g_1}({}^{I_1}\dot{\boldsymbol{\omega}} \times {}^1\mathbf{p}_2) + {}^1\mathbf{C}_2\mathbf{S}_{g_2}^{-1}\mathbf{S}_{g_2}({}^{I_2}\dot{\boldsymbol{\omega}} \times {}^2\mathbf{p}_1) \\ \mathbf{K}_k\mathbf{S}_{g_1}^{-1}\mathbf{S}_{g_1}({}^{I_1}\dot{\boldsymbol{\omega}} \times {}^1\mathbf{p}_2) \end{bmatrix} \tag{88}$$

$$= \begin{bmatrix} ({}^{I_1}\dot{\boldsymbol{\omega}} \times {}^1\mathbf{p}_2) + {}^1\mathbf{C}_2({}^{I_2}\dot{\boldsymbol{\omega}} \times {}^2\mathbf{p}_1) \\ \mathbf{K}_k({}^{I_1}\dot{\boldsymbol{\omega}} \times {}^1\mathbf{p}_2) \end{bmatrix} \tag{89}$$

$$= \begin{bmatrix} \mathbf{0}_{3\times1} \\ (\lfloor {}^{I_1}\boldsymbol{\omega}_k \times {}^1\mathbf{p}_2\rfloor + \lfloor {}^{I_1}\boldsymbol{\omega}_k\rfloor\lfloor {}^1\mathbf{p}_2\rfloor)\,({}^{I_1}\dot{\boldsymbol{\omega}} \times {}^1\mathbf{p}_2) \end{bmatrix} \tag{90}$$

when (34) is satisfied, ${}^{I_1}\boldsymbol{\omega}_k \parallel {}^{I_1}\dot{\boldsymbol{\omega}}$ and ${}^{I_1}\boldsymbol{\omega}_k \perp {}^1\mathbf{p}_2$, according to Lemma 1, we have:

$$\Leftrightarrow \mathbf{M}_k\mathbf{N}_{\mathbf{b}_g^+\perp} = \mathbf{0}_{6\times1} \tag{91}$$

B. Verification of Unobservable Direction $\mathbf{N}_{\mathbf{s}_g^+,\mathbf{b}_a\perp}$

$$\mathbf{M}_k\mathbf{N}_{\mathbf{s}_g^+,\mathbf{b}_a\perp} = \begin{bmatrix} -\mathbf{S}_{g_1}^{-1} & {}^1\mathbf{C}_2\mathbf{S}_{g_2}^{-1} & -\mathbf{\Lambda}({}^{I_1}\boldsymbol{\omega}_k)\mathbf{S}_{g_1}^{-1} & {}^1\mathbf{C}_2\mathbf{\Lambda}({}^{I_2}\boldsymbol{\omega}_k)\mathbf{S}_{g_2}^{-1} & \mathbf{0}_3 & \mathbf{0}_3 \\ -\mathbf{K}_k\mathbf{S}_{g_1}^{-1} & \mathbf{0}_3 & -\mathbf{L}_k\mathbf{S}_{g_1}^{-1} & \mathbf{0}_3 & \mathbf{I}_3 & -{}^1\mathbf{C}_2 \end{bmatrix} \begin{bmatrix} \mathbf{0}_{6\times1} \\ -\mathbf{S}_{g_1}\mathbf{\Lambda}({}^{I_1}\dot{\boldsymbol{\omega}})^{-1}({}^{I_1}\dot{\boldsymbol{\omega}}\times{}^1\mathbf{p}_2) \\ \mathbf{S}_{g_2}\mathbf{\Lambda}({}^{I_2}\dot{\boldsymbol{\omega}})^{-1}({}^{I_2}\dot{\boldsymbol{\omega}}\times{}^2\mathbf{p}_1) \\ -\mathbf{L}_1\mathbf{\Lambda}({}^{I_2}\dot{\boldsymbol{\omega}})^{-1}({}^{I_1}\dot{\boldsymbol{\omega}}\times{}^1\mathbf{p}_2) \\ \mathbf{0}_{3\times1} \end{bmatrix} \tag{92}$$

$$= \begin{bmatrix} \mathbf{\Lambda}({}^{I_1}\boldsymbol{\omega}_k)\mathbf{S}_{g_1}^{-1}\mathbf{S}_{g_1}\mathbf{\Lambda}({}^{I_1}\dot{\boldsymbol{\omega}})^{-1}({}^{I_1}\dot{\boldsymbol{\omega}}\times{}^1\mathbf{p}_2) + {}^1\mathbf{C}_2\mathbf{\Lambda}({}^{I_2}\boldsymbol{\omega}_k)\mathbf{S}_{g_2}^{-1}\mathbf{S}_{g_2}\mathbf{\Lambda}({}^{I_2}\dot{\boldsymbol{\omega}})^{-1}({}^{I_2}\dot{\boldsymbol{\omega}}\times{}^2\mathbf{p}_1) \\ \mathbf{L}_k\mathbf{S}_{g_1}^{-1}\mathbf{S}_{g_1}\mathbf{\Lambda}({}^{I_1}\dot{\boldsymbol{\omega}})^{-1}({}^{I_1}\dot{\boldsymbol{\omega}}\times{}^1\mathbf{p}_2) - \mathbf{L}_1\mathbf{\Lambda}({}^{I_1}\dot{\boldsymbol{\omega}})^{-1}({}^{I_1}\dot{\boldsymbol{\omega}}\times{}^1\mathbf{p}_2) \end{bmatrix} \tag{93}$$

$$= \begin{bmatrix} \mathbf{\Lambda}({}^{I_1}\boldsymbol{\omega}_k)\mathbf{\Lambda}({}^{I_1}\dot{\boldsymbol{\omega}})^{-1}({}^{I_1}\dot{\boldsymbol{\omega}}\times{}^1\mathbf{p}_2) + {}^1\mathbf{C}_2\mathbf{\Lambda}({}^{I_2}\boldsymbol{\omega}_k)\mathbf{\Lambda}({}^{I_2}\dot{\boldsymbol{\omega}})^{-1}({}^{I_2}\dot{\boldsymbol{\omega}}\times{}^2\mathbf{p}_1) \\ (\mathbf{L}_k-\mathbf{L}_1)\mathbf{\Lambda}({}^{I_1}\dot{\boldsymbol{\omega}})^{-1}({}^{I_1}\dot{\boldsymbol{\omega}}\times{}^1\mathbf{p}_2) \end{bmatrix} \tag{94}$$

when (34) is satisfied, ${}^{I_1}\boldsymbol{\omega}_k \parallel {}^{I_1}\dot{\boldsymbol{\omega}}$ and ${}^{I_2}\boldsymbol{\omega}_k \parallel {}^{I_2}\dot{\boldsymbol{\omega}}$, we have:

$$\mathbf{\Lambda}({}^{I_1}\boldsymbol{\omega}_k)\mathbf{\Lambda}({}^{I_1}\dot{\boldsymbol{\omega}})^{-1} = \mathbf{\Lambda}({}^{I_2}\boldsymbol{\omega}_k)\mathbf{\Lambda}({}^{I_2}\dot{\boldsymbol{\omega}})^{-1} \tag{95}$$

$$= \frac{\|{}^{I_1}\boldsymbol{\omega}_k\|}{\|{}^{I_1}\dot{\boldsymbol{\omega}}\|} = \frac{\|{}^{I_2}\boldsymbol{\omega}_k\|}{\|{}^{I_2}\dot{\boldsymbol{\omega}}\|} \triangleq \alpha_k \tag{96}$$

$$\Leftrightarrow \mathbf{M}_k\mathbf{N}_{\mathbf{s}_g^+,\mathbf{b}_a\perp} = \begin{bmatrix} \alpha_k(({}^{I_1}\dot{\boldsymbol{\omega}}\times{}^1\mathbf{p}_2) + {}^1\mathbf{C}_2({}^{I_2}\dot{\boldsymbol{\omega}}\times{}^2\mathbf{p}_1)) \\ (\mathbf{L}_k-\mathbf{L}_1)\mathbf{\Lambda}({}^{I_1}\dot{\boldsymbol{\omega}})^{-1}({}^{I_1}\dot{\boldsymbol{\omega}}\times{}^1\mathbf{p}_2) \end{bmatrix} \tag{97}$$

$$= \begin{bmatrix} \mathbf{0}_{3\times1} \\ (\mathbf{L}_k-\mathbf{L}_1)\mathbf{\Lambda}({}^{I_1}\dot{\boldsymbol{\omega}})^{-1}({}^{I_1}\dot{\boldsymbol{\omega}}\times{}^1\mathbf{p}_2) \end{bmatrix} \tag{98}$$

Applying (22) yields:

$$\Leftrightarrow \mathbf{M}_k\mathbf{N}_{\mathbf{s}_g^+,\mathbf{b}_a\perp} = \begin{bmatrix} \mathbf{0}_{3\times1} \\ \left(\mathbf{K}_k\mathbf{\Lambda}({}^{I_1}\boldsymbol{\omega}_k) + \lfloor{}^1\mathbf{p}_2\rfloor\mathbf{\Lambda}({}^{I_1}\dot{\boldsymbol{\omega}}_k) - \mathbf{K}_1\mathbf{\Lambda}({}^{I_1}\boldsymbol{\omega}_1) - \lfloor{}^1\mathbf{p}_2\rfloor\mathbf{\Lambda}({}^{I_1}\dot{\boldsymbol{\omega}}_1)\right)\mathbf{\Lambda}({}^{I_1}\dot{\boldsymbol{\omega}})^{-1}({}^{I_1}\dot{\boldsymbol{\omega}}\times{}^1\mathbf{p}_2) \end{bmatrix} \tag{99}$$

From (34), we have ${}^{I_1}\dot{\boldsymbol{\omega}}_1 = {}^{I_1}\dot{\boldsymbol{\omega}}_k$, hence:

$$\Leftrightarrow \mathbf{M}_k\mathbf{N}_{\mathbf{s}_g^+,\mathbf{b}_a\perp} = \begin{bmatrix} \mathbf{0}_{3\times1} \\ \mathbf{K}_k\mathbf{\Lambda}({}^{I_1}\boldsymbol{\omega}_k)\mathbf{\Lambda}({}^{I_1}\dot{\boldsymbol{\omega}})^{-1}({}^{I_1}\dot{\boldsymbol{\omega}}\times{}^1\mathbf{p}_2) - \mathbf{K}_1\mathbf{\Lambda}({}^{I_1}\boldsymbol{\omega}_1)\mathbf{\Lambda}({}^{I_1}\dot{\boldsymbol{\omega}})^{-1}({}^{I_1}\dot{\boldsymbol{\omega}}\times{}^1\mathbf{p}_2) \end{bmatrix} \tag{100}$$

$$= \begin{bmatrix} \mathbf{0}_{3\times1} \\ \alpha_k\mathbf{K}_k({}^{I_1}\dot{\boldsymbol{\omega}}\times{}^1\mathbf{p}_2) - \alpha_1\mathbf{K}_1({}^{I_1}\dot{\boldsymbol{\omega}}\times{}^1\mathbf{p}_2) \end{bmatrix} \tag{101}$$

Similar to equation (89), we have $\mathbf{K}_k({}^{I_1}\dot{\boldsymbol{\omega}}\times{}^1\mathbf{p}_2) = \mathbf{0}_{3\times1}$ for any $k = 1, 2, \cdots$, hence:

$$\Leftrightarrow \mathbf{M}_k\mathbf{N}_{\mathbf{s}_g^+,\mathbf{b}_a\perp} = \mathbf{0}_{6\times1} \tag{102}$$

REFERENCES

[1] E.-H. Shin and N. El-Sheimy, "Accuracy improvement of low cost ins/gps for land applications," in *Proc. of the national technical meeting of the institute of navigation*, 2002, pp. 146–157.

[2] F. Caron, E. Duflos, D. Pomorski, and P. Vanheeghe, "Gps/imu data fusion using multisensor kalman filtering: introduction of contextual aspects," *Information fusion*, vol. 7, no. 2, pp. 221–230, 2006.

[3] A. I. Mourikis and S. I. Roumeliotis, "A multi-state constraint kalman filter for vision-aided inertial navigation," in *Proc. of the IEEE International Conference on Robotics and Automation (ICRA)*, 2007, pp. 3565–3572.

[4] T. Qin, P. Li, and S. Shen, "Vins-mono: A robust and versatile monocular visual-inertial state estimator," *IEEE Transactions on Robotics*, vol. 34, no. 4, pp. 1004–1020, August 2018.

[5] S. Leutenegger, S. Lynen, M. Bosse, R. Siegwart, and P. Furgale, "Keyframe-based visual–inertial odometry using nonlinear optimization," *The International Journal of Robotics Research*, vol. 34, no. 3, pp. 314–334, 2015.

[6] P. Geneva, K. Eckenhoff, W. Lee, Y. Yang, and G. Huang, "Openvins: A research platform for visual-inertial estimation," in *Proc. of the IEEE International Conference on Robotics and Automation (ICRA)*, 2020, pp. 4666–4672.

[7] R. Mur-Artal and J. D. Tardós, "Visual-inertial monocular slam with map reuse," *IEEE Robotics and Automation Letters*, vol. 2, no. 2, pp. 796–803, February 2017.

[8] K. Wu, A. M. Ahmed, G. A. Georgiou, and S. I. Roumeliotis, "A square root inverse filter for efficient vision-aided inertial navigation on mobile devices," in *Robotics: Science and Systems Conference (RSS)*, vol. 2, 2015, p. 2.

[9] T. Shan, B. Englot, D. Meyers, W. Wang, C. Ratti, and D. Rus, "Lio-sam: Tightly-coupled lidar inertial odometry via smoothing and mapping," in *Proc. of the IEEE/RSJ International Conference on Intelligent Robots and Systems (IROS)*, 2020, pp. 5135–5142.

[10] W. Xu and F. Zhang, "Fast-lio: A fast, robust lidar-inertial odometry package by tightly-coupled iterated kalman filter," *IEEE Robotics and Automation Letters*, vol. 6, no. 2, pp. 3317–3324, 2021.

[11] M. Zhang, X. Xu, Y. Chen, and M. Li, "A lightweight and accurate localization algorithm using multiple inertial measurement units," *IEEE Robotics and Automation Letters*, vol. 5, no. 2, pp. 1508–1515, January 2020.

[12] K. Eckenhoff, P. Geneva, and G. Huang, "Mimc-vins: A versatile and resilient multi-imu multi-camera visual-inertial navigation system," *IEEE Transactions on Robotics*, vol. 37, no. 5, pp. 1360–1380, February 2021.

[13] A. Jadid, L. Rudolph, F. Pankratz, and G. Klinker, "Utilizing multiple calibrated imus for enhanced mixed reality tracking," in *Proc. of the IEEE International Symposium on Mixed and Augmented Reality Adjunct (ISMAR-Adjunct)*, 2019, pp. 384–386.

[14] R. Zhang, F. Hoflinger, and L. M. Reind, "Calibration of an imu using 3-d rotation platform," *IEEE sensors Journal*, vol. 14, no. 6, pp. 1778–1787, January 2014.

[15] S. Y. Cho and C. G. Park, "A calibration technique for a redundant imu containing low-grade inertial sensors," *ETRI journal*, vol. 27, no. 4, pp. 418–426, August 2005.

[16] A. Kim and M. Golnaraghi, "Initial calibration of an inertial measurement unit using an optical position tracking system," in *Proc. of the the Position Location and Navigation Symposium (PLANS)*, 2004, pp. 96–101.

[17] C. Le Gentil and T. Vidal Calleja, "A gaussian process approach for imu to pose spatiotemporal calibration," in *Proc. of the Australasian Conference on Robotics and Automation*, 2023.

[18] J. Rehder, J. Nikolic, T. Schneider, T. Hinzmann, and R. Siegwart, "Extending kalibr: Calibrating the extrinsics of multiple imus and of individual axes," in *Proc. of the IEEE International Conference on Robotics and Automation (ICRA)*, 2016, pp. 4304–4311.

[19] D. Zachariah and M. Jansson, "Joint calibration of an inertial measurement unit and coordinate transformation parameters using a monocular camera," in *Proc. of the IEEE International Conference on Indoor Positioning and Indoor Navigation*, 2010, pp. 1–7.

[20] Y. Yang, P. Geneva, and G. Huang, "Multi-visual-inertial system: Analysis, calibration, and estimation," *The International Journal of Robotics Research*, 2024.

[21] J. Rehder and R. Siegwart, "Camera/imu calibration revisited," *IEEE Sensors Journal*, vol. 17, no. 11, pp. 3257–3268, February 2017.

[22] Y. Yang, P. Geneva, X. Zuo, and G. Huang, "Online self-calibration for visual-inertial navigation: Models, analysis, and degeneracy," *IEEE Transactions on Robotics*, vol. 39, no. 5, pp. 3479–3498, June 2023.

[23] Y. Yu, Y. Liu, F. Fu, S. He, D. Zhu, L. Wang, X. Zhang, and J. Li, "Fast extrinsic calibration for multiple inertial measurement units in visual-inertial system," in *Proc. of the IEEE International Conference on Robotics and Automation (ICRA)*, 2023, pp. 01–07.

[24] J. Lv, X. Zuo, K. Hu, J. Xu, G. Huang, and Y. Liu, "Observability-aware intrinsic and extrinsic calibration of lidar-imu systems," *IEEE Transactions on Robotics*, vol. 38, no. 6, pp. 3734–3753, June 2022.

[25] D. Tedaldi, A. Pretto, and E. Menegatti, "A robust and easy to implement method for imu calibration without external equipments," in *Proc. of the IEEE International Conference on Robotics and Automation (ICRA)*, 2014, pp. 3042–3049.

[26] J. Rohac, M. Sipos, and J. Simanek, "Calibration of low-cost triaxial inertial sensors," *IEEE Instrumentation & Measurement Magazine*, vol. 18, no. 6, pp. 32–38, November 2015.

[27] I. Frosio, F. Pedersini, and N. A. Borghese, "Autocalibration of mems accelerometers," *IEEE Transactions on Instrumentation and Measurement*, vol. 58, no. 6, pp. 2034–2041, October 2008.

[28] W. Fong, S. Ong, and A. Nee, "Methods for in-field user calibration of an inertial measurement unit without external equipment," *Measurement Science and technology*, vol. 19, no. 8, p. 085202, July 2008.

[29] J. Lee, D. Hanley, and T. Bretl, "Extrinsic calibration of multiple inertial sensors from arbitrary trajectories," *IEEE Robotics and Automation Letters*, vol. 7, no. 2, pp. 2055–2062, January 2022.

[30] D. Kim, S. Shin, and I. S. Kweon, "On-line initialization and extrinsic calibration of an inertial navigation system with a relative preintegration method on manifold," *IEEE transactions on Automation Science and Engineering*, vol. 15, no. 3, pp. 1272–1285, December 2017.

[31] P. Schopp, H. Graf, W. Burgard, and Y. Manoli, "Self-calibration of accelerometer arrays," *IEEE Transactions on Instrumentation and Measurement*, vol. 65, no. 8, pp. 1913–1925, April 2016.

[32] T. Wang and S. I. Roumeliotis, "A direct algorithm for multi-gyroscope infield calibration," *arXiv preprint arXiv:2403.08177*, 2024.

[33] K. J. Wu, C. X. Guo, G. Georgiou, and S. I. Roumeliotis, "Vins on wheels," in *Proc. of the IEEE International Conference on Robotics and Automation (ICRA)*, 2017, pp. 5155–5162.

[34] T. Schneider, M. Li, C. Cadena, J. Nieto, and R. Siegwart, "Observability-aware self-calibration of visual and inertial sensors for ego-motion estimation," *IEEE Sensors Journal*, vol. 19, no. 10, pp. 3846–3860, January 2019.

[35] A. Martinelli, "Vision and imu data fusion: Closed-form solutions for attitude, speed, absolute scale, and bias determination," *IEEE Transactions on Robotics*, vol. 28, no. 1, pp. 44–60, July 2011.

[36] W. Lai, R. Guo, and K. J. Wu, "Dual-imu state estimation for relative localization of two mobile agents," in *Proc. of the IEEE International Conference on Robotics and Automation (ICRA)*, 2024, pp. 11 927–11 933.

[37] S. Agarwal, K. Mierle, and T. C. S. Team, "Ceres Solver," October 2023. [Online]. Available: https://github.com/ceres-solver/ceres-solver

[38] Z. Chen, K. Jiang, and J. C. Hung, "Local observability matrix and its application to observability analyses," in *Proc. of the IECON'90: 16th Annual Conference of IEEE Industrial Electronics Society*, 1990, pp. 100–103.

[39] G. Strang, *Introduction to linear algebra*. SIAM, 2022.